1998

Characterization and Analysis of the Superabrasive Diamond Blade Sawing Process.

Harlan Dwayne Jerro
Louisiana State University and Agricultural & Mechanical College

INFORMATION TO USERS

This manuscript has been reproduced from the microfilm master. UMI films the text directly from the original or copy submitted. Thus, some thesis and dissertation copies are in typewriter face, while others may be from any type of computer printer.

The quality of this reproduction is dependent upon the quality of the copy submitted. Broken or indistinct print, colored or poor quality illustrations and photographs, print bleedthrough, substandard margins, and improper alignment can adversely affect reproduction.

In the unlikely event that the author did not send UMI a complete manuscript and there are missing pages, these will be noted. Also, if unauthorized copyright material had to be removed, a note will indicate the deletion.

Oversize materials (e.g., maps, drawings, charts) are reproduced by sectioning the original, beginning at the upper left-hand corner and continuing from left to right in equal sections with small overlaps. Each original is also photographed in one exposure and is included in reduced form at the back of the book.

Photographs included in the original manuscript have been reproduced xerographically in this copy. Higher quality 6" x 9" black and white photographic prints are available for any photographs or illustrations appearing in this copy for an additional charge. Contact UMI directly to order.

UMI

A Bell & Howell Information Company
300 North Zeeb Road, Ann Arbor MI 48106-1346 USA
313/761-4700 800/521-0600

CHARACTERIZATION AND ANALYSIS OF THE SUPERABRASIVE DIAMOND BLADE SAWING PROCESS

A Dissertation

Submitted to the Graduate Faculty of the
Louisiana State University and
Agricultural and Mechanical College
in partial fulfillment of the
requirements for the degree of
Doctor of Philosophy

in

The Department of Mechanical Engineering

by
Harlan Dwayne Jerro
B.S., Southern University and A & M College, 1991
December 1998

ACKNOWLEDGMENTS

I would like to thank God for giving me the opportunity, ability, and strength to to undertake the task which is presented in this dissertation and to complete graduate school. First, it is to Him and his son, Jesus, that I dedicate this work. Second, I dedicate this work to the memory of my mother, Annette Jerro, better known as Deah, who passed last year (December 1997). She always taught me to work hard, never quit, and love God, people, and life with all my heart. Her memory is ever in my heart, and we will truly miss the light she brought to our life.

I would like to thank my beautiful wife, Valerie, for her never-ending patience with me and this "chapter" of my life. Truly you are the apple of my eye. I love you and am thankful for you. I also acknowledge and thank my father, Walter Jerro, Jr., my sister, Nina, and brother, Cappy, their families, and my other immediate and extended family members and friends. I would have never completed this task without all of your love, prayers, and support.

I also thank all of my graduate committee members - Dr. Su-Seng Pang, Dr. C. Charles Yang, Dr. George Z. Voyiadjis, Dr. Reza Mirshams, Dr. T. Warren Liao, Dr. Mehdy Sabbaghian, and Dr. John R. Collier - for your guidance, support, and assistance. Foremost, I want to thank Dr. Pang for his tremendous tutelage and leadership over these past seven years. I also thank all of my friends and colleagues in the Composite Materials Laboratory and the Mechanical Engineering Model Shop, and Mr. Willie Dillworth for their help and encouragement. I also thank Mr. Massoud Besharat at Imex

International, Dr. Steven Hayden at General Electric Superabrasives, and Mr. Zak Asmelash and Mr. Metin Sakarcan at Diamond Boart, Inc. for their help.

Finally, part of my work was sponsored by the Louisiana Board of Regents under the LEQSF PLEx program and IMEX International (formerly, SEA Diamond Tools, U.S.A., Inc.), Elberton, GA. I would like to express thanks to these organizations. I also acknowledge and thank the Louisiana Board of Regents for their Doctoral Fellowship support, the Huel D. Perkins Doctoral Fellowship Committee, and the LSU Graduate School for their fellowship and tuition support during a portion of my stay at LSU.

TABLE OF CONTENTS

ABSTRACT

Diamond-impregnated segmented circular blade sawing is one of the most effective, versatile, and extensively used methods of processing rock and other hard materials, such as granite, marble, concrete and asphalt. For many years, it has been known that chip thickness is one of the most significant parameters in the understanding of the sawing process, and other variables such as force and power have been correlated with it.

In this work, the material chipping geometries have been mathematically defined and derived through kinematics analysis. From these chipping geometries, chip area and thickness relations have been obtained. A relation for the mean chip thickness-to-grit spacing ratio has also been obtained as a function of independent non-dimensional machining parameter ratios. The effects of these independent non-dimensional parameters on the mean thickness were also investigated. The results show an excellent agreement between the new chipping model and the older ones. However, at moderately small to large depth of cut to blade diameter ratios values, the new model yields a more exact result.

The grit spacing parameter used in the mean chip thickness-to-grit spacing ratio equation has also been examined. Methods were formulated to (a) analytically and (b) numerically compute an explicit value for the grit spacing. A comparison has also been made to verify the results for the grit spacing term. The results showed excellent agreement between the presented models and experimental data.

Finally, the stress distribution of the segmented blade was investigated through the use of finite element analysis. Saw blades with various slot parameters were investigated and compared. The applied forces included the saw blade cutting force as well as the centrifugal force due to rotation. Plane stress conditions were assumed during the investigation. The maximum stress for each geometry was located and its magnitude was determined. In summary, an improved slot shape has been suggested to minimize the stress concentration and thereby increase the saw blade fatigue life.

CHAPTER 1

INTRODUCTION

1.1 Background

Superabrasive diamond sawing can be classified as a hybrid machining process. For it is a combination of the conventional milling or wood sawing processes and the grinding process. This is true because it uses small to fairly large sized blades to remove material from a workpiece. The amount of material removed during one cutting pass may be relatively large or small, as seen in grinding and/or material finishing.

Diamond tools play a vital role in the stone and construction industries. These industries, as well as the diamond tool industry, have grown as a result of vast improvements in the abrasive materials, tool fabrication, and joining methods. These and other factors have substantially improved productivity and lowered costs in the stone and construction industries (Konstanty, 1991). Thus, diamond tools have presently proven themselves to be practical and feasible alternatives to conventional tooling methods. Furthermore, circular sawing is one of the most effective, versatile, and extensively used methods of processing of rock and other hard materials such as concrete and asphalt (Pai et al., 1988). The stone processing industry represents one of the largest users of industrial diamonds worldwide (Burgess and Birle, 1978).

Today an increasing number of architects and mining and construction engineers utilize diamond tools in their work because they know that these tools are faster and easier to use than older, conventional tools such as sledge hammers and pneumatic and

hydraulic jacks. Diamond tools are preferred for use in renovating buildings because they have low dust and noise levels, produce clean and precise cuts, and do not cause vibrations that may lead to structural damage (e.g., cracks) which normal methods can cause. Therefore, work can proceed both inside and outside of a building with minimal disruption to its inhabitants and the general public, as well as minimal additional repairs (Wilks and Wilks, 1991). In the mining and stone-processing industries, diamond saw blades and wire saws are used to remove hard rocks from quarries and then to cut these rocks once they are removed. Diamond asphalt and concrete cutting machines are used to cut bridge and highway surfaces to enable rapid, clean, and easy section removal and replacement. Since the use of diamond tools requires less time and manpower, the overall cost is lowered.

Furthermore, there has also been a significant effort to improve the range and performance of cutting tool materials available to production, manufacturing, mining, and civil engineers. The nature of the materials cut in the stone and construction industries, such as granite and concrete, requires super-hard tooling materials. Current research and development in the area of superabrasive diamond tools contribute significantly to providing better cutting tools for such materials.

1.2 Goal and Scope of Work

As mentioned above, diamond tools have many advantages; however, some limitations still exist. There has been a need for fundamental research on the cutting mechanism (or process) of the circular diamond saw blade. Currently, work has been underway to develop a better model for the cutting process. It is believed that future prosperity in this industry lies in the ability to characterize and fine tune the

manufacturing process of sawing. Therefore, one of the primary goals of diamond tools research is to characterize the diamond-cutting process analytically, numerically, and experimentally. Therefore, the basis and purpose of this work is to provide fundamental tools for the advancement of the superabrasive diamond sawing process by providing realistic models of the sawing process. As result of such characterization work, other useful by-products can also be developed. End-users of such a model (or black box) can use it in conjunction with other tools, such as optimization software, to perform numerical optimizations without performing expensive and rigorous iterations of trial and error experiments.

The major elements of this work are threefold. First, a new analytical kinematics model is presented in Chapter 2 to describe the position, displacement, and motion attributes of the machining process. From this model, important machining parameters are derived, such as the mean chip thickness, t_c, and the mean chip thickness-to-grit spacing ratio, t_c/λ. In Chapter 3, a grit distribution model is developed which addresses the very complex and random aspects of the diamond tool surface. The model develops analytical and numerical methods to compute the grit spacing parameter, λ. Finally, Chapter 4 discusses the optimization of the blade design by studying the stresses developed during the sawing process. This optimization procedure is implemented by using the finite element method (FEM). From this analysis it is shown that maximum stresses induced during sawing can be minimized by changing the blade design.

CHAPTER 2

KINEMATIC ANALYSIS

A kinematics analysis of a material chipped by a single grit of the saw blade is now undertaken. In this analysis, the derived mathematical relations of the chipping geometry are based solely on the independent machining parameters. The chipping geometry parameters derived are important since past research in the grinding field has indicated that chip thickness, t_c, is proportional to the relative chip-cutting force, f_r, by some factor, n

$$t_c^n = f_r \tag{2.1}$$

This factor, n, has been estimated to have a value between 1 and 2 (Reichenbach et al., 1956; Kalpakjian, 1984; McGowan and Brauninger, 1991). To evaluate the relevance of the proposed model, a comparison will be made with former chip thickness models.

2.1 Diamond Saw Blade Cutting System

The diamond blade cutting system consists of the following parts: (1) The cutting machine, which provides rigidity and structural stability as well as its operating capability, (2) the workpiece, which is being cut and provides the resistance to the blade, and (3) the cutting blade, which provides the necessary hardness and strength for the cutting process. For this study, the workpiece material is granite rock.

The circular diamond saw blade consists of two major components: (a) the diamond segment and (b) the blade core (or hub). The diamond segment is a composite material composed of diamond particles, ranging from 150 to 1000 μm in diameter,

dispersed in a metal matrix binder. The metal matrix material initially consists of very fine powder particles (approximately 0.5 to 2 μm). Typical matrix materials include cobalt, bronze, and tungsten carbide. Generally, segment manufacturers use "shakers" which mix the diamond grits with the matrix material's particles for an extended length of time (on the order of hours) to ensure a good random distribution of particles. After mixing is completed, the mixture of diamonds and metal matrix particles are sintered using either hot or cold pressing methods. After all of the processing is completed, these grits are randomly distributed throughout the segment. Theoretically, this means that at any given time the surface of the segment will consist of randomly located grits at random relative heights of protrusion from the matrix surface. It should also be noted that because of the vast size difference between matrix particles and grits, obtaining a random distribution has posed a problem for segment manufacturers in the past. But with manufacturing skill and care, a fairly good (random) distribution can be obtained.

Usually, the diamond segments are manufactured in rectangular blocks with a range of lengths (L_{seg}), typically between 20 to 50 mm. This segment is normally mounted to the periphery of a very thin steel blade core, with thickness values on the order of several millimeters, with a slot (or gap) between each segment. Adding the circumferential distance of this slot (L_{slot}) to the segment length gives the value of the segment pitch (L_p). Nominal blade diameters generally range from 200 mm to 3 m (Wilks and Wilks, 1991; Mahomed et al, 1972; Büttner, 1974).

Figure 2.1 gives an illustration of a typical cutting process with a diamond blade. The following parameters have a direct relation to the chipping geometries:

h: Depth of cut

D: Blade diameter

v_T: Traverse rate

v_P: Peripheral speed of the diamond blade

λ: Circumferential distance between the first and second diamond grits, measured along the diamond blade periphery.

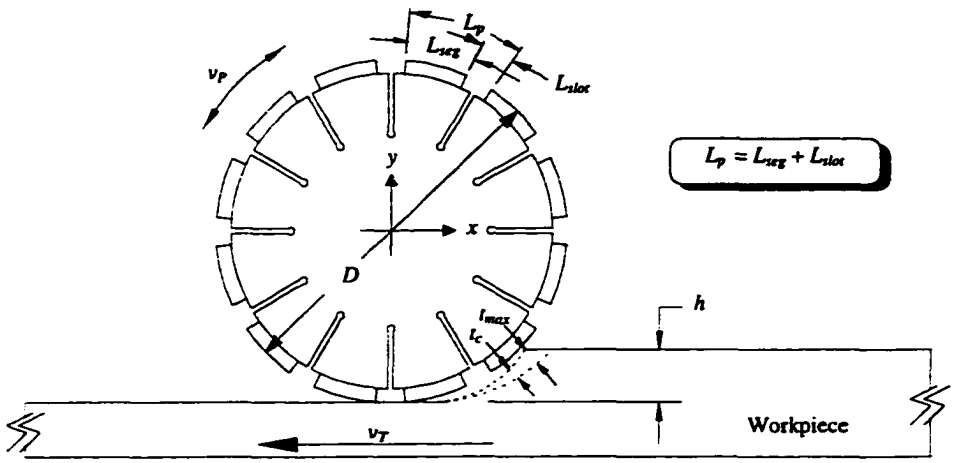

Figure 2.1 Diamond Blade Cutting System. This figure illustrates the slotted steel blade, diamond segments, and the workpiece material.

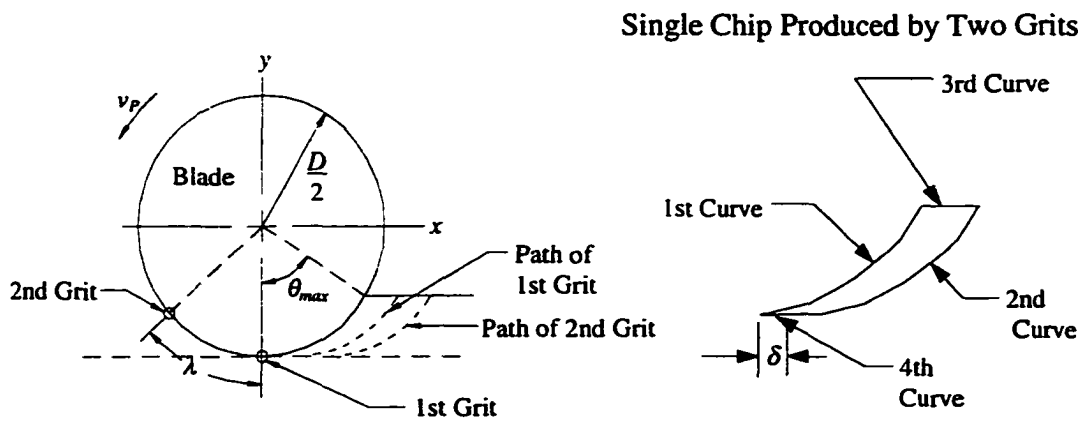

Figure 2.2 The above illustration to the left shows grit path taken by two successive "in-line" diamond grits and the spacing λ between them. The illustration on the right shows the workpiece material region (i.e., the chip) bounded by the two grits and the workpiece surfaces.

2.2 Cutting Process and Chip Formation Phenomenon

The saw blade rotates about the blade center with an angular speed and cuts into the workpiece at a constant traverse rate. The diamond particles on the segment surface remove material through scratching and cracking the workpiece surface. During these processes it has been observed that the formation of chips accompanies the deformation and parting of the workpiece material. Some researchers have used the chip area parameter (A_c) as a means to characterize the chip formation process (Büttner, 1974; Ertingshausen, 1985). But according to many researchers, the decisive factor affecting the mechanical processes during the diamond sawing operation is chip formation, which is characterized by the chip thickness parameter (Tönshoff and Warnecke, 1982; Brecker and Shaw, 1974). According to Pai (1987), the chip thickness parameter is important because it determines the contact stresses on the grit, thereby influencing the required bond strength. The energy consumed per unit volume of material removed (or specific energy) in grinding has been found to be a strong function of the maximum chip thickness (Reichenbach et al., 1956). Furthermore, the specific energy determines the cutting temperatures, which influence the wear and surface integrity.

Corresponding to the chipping process are complex compressive and shear stresses which are developed along the diamond segment and workpiece surfaces. These stresses are distributed throughout the saw blade, diamond segment, and workpiece, and they are usually quite large near the cutting surface due to the small surface contact area(s). The complexity of the stresses stems from the cutting forces. These forces are affected by many, if not all, of the independent machining parameters and the workpiece material properties.

As shown in Figure 2.2, two successive diamond grit attachments will remove a chip of material through the scratching and cracking processes previously mentioned. Thus, the forces acting at the cutting point are determined by this newly formed chip. With the definition given above, it can be seen that a mathematical expression of the chip can be obtained, by which the chip is defined by the region enclosed by the intersection of all four curves. This expression will be related to each parameter mentioned in Figure 2.1. The first curve is the trace of the first diamond grit, the second curve is the trace of the second diamond grit, the third is the workpiece surface before cutting, while the fourth is the machined surface after cutting. In order to determine the area of each chip and the chip thickness, the mathematical relationships of these four curves will be derived below.

2.3 Chip Geometry Development of the Diamond Sawing Operation

2.3.1 Mathematical Expressions of Chip Curves

The motion of the first grit represents the relative motion of the grit relative to the workpiece. The grit rotates about the blade center with the angular velocity ω of the saw blade. If the origin of the absolute coordinate system is defined to be the blade's center (which is fixed), the grit trajectory can be defined as:

$$\vec{f}_{1g} = \frac{D}{2}\sin\omega t\ \hat{i} - \frac{D}{2}\cos\omega t\ \hat{j} \tag{2.2}$$

where, $\omega = 2v_P/D$.

The motion of the workpiece is caused by the transverse velocity, v_T, and is defined as:

$$\vec{f}_{1w} = -v_T t\ \hat{i} \tag{2.3}$$

Therefore, the expression of the first diamond grit can be obtained as:

$$\begin{aligned}\vec{f}_1 &= \vec{f}_{1g} - \vec{f}_{1w} \\ &= \left(v_T t + \frac{D}{2}\sin\omega t\right)\hat{i} - \frac{D}{2}\cos\omega t\,\hat{j}\end{aligned} \tag{2.4}$$

The second grit trajectory is identical to the first grit, except for being horizontally offset by a distance, δ, shown in Figure 2.2. This parameter can be related to v_T, λ, ω, and D as follows:

The time, τ, required for the second grit to reach the bottom surface is:

$$\tau = \frac{2\lambda}{\omega D} = \frac{\lambda}{v_P} \tag{2.5}$$

and thus,

$$\delta = v_T\tau = v_T\frac{2\lambda}{\omega D} \tag{2.6}$$

The third and fourth curves of the chipped material shown in Figure 2.2 are obvious and have been defined.

2.3.2 Chip Thickness

Referring to Eq. (2.4), the first grit's trajectory can be expressed in terms of the Cartesian coordinates, x and y, as follows:

$$x = v_T t + \frac{D}{2}\sin\omega t \tag{2.7}$$

$$y = -\frac{D}{2}\cos\omega t \tag{2.8}$$

The chip arc length, S, defined by the first grit can be obtained as follows:

$$S = \int ds = \int_{t_0}^{t_1}\sqrt{(dx/dt)^2 + (dy/dt)^2}\,dt \tag{2.9}$$

and using the derivatives from Eqs. (2.7) and (2.8), an expression for the chip arc length can be obtained

$$S = \int_{t_0}^{t_1} \sqrt{v_T^2 + \frac{D^2\omega^2}{4} + v_T D\omega \cos\omega t}\, dt \tag{2.10}$$

The lower integration limit t_0 is 0 while the upper integration limit is

$$t_1 = \frac{1}{\omega}\cos^{-1}\left(1 - \frac{2h}{D}\right) \tag{2.11}$$

This integral expression can be rewritten by transforming the variable t and its differential, dt, into Φ and $d\Phi$, respectively, by the equations

$$\Phi = \frac{\omega}{2}t \qquad \text{and} \qquad d\Phi = \frac{\omega}{2}dt = \frac{v_P}{D}dt \tag{2.12}$$

and introducing two new variables, the depth of cut to blade diameter ratio, K_1, and the transverse to peripheral speed ratio K_2 (hereafter called the depth-diameter ratio and speed ratio, respectively), where

$$K_1 = \frac{h}{D} \qquad \text{and} \qquad K_2 = \frac{v_T}{v_P} \tag{2.13}$$

The function in the integral underneath the square root sign can also be rewritten as

$$v_T^2 + \frac{D^2\omega^2}{4} + v_T D\omega\cos\omega t = v_T^2 + v_P^2 + 2v_T v_P \cos\omega t \tag{2.14}$$

Now, multiplying this expression on the right side of the equal sign by $(v_P/v_P)^2$, which is unity, yields

$$\begin{aligned} v_T^2 + v_P^2 + 2v_T v_P\cos\omega t &= (v_P/v_P)^2\left(v_T^2 + v_P^2 + 2v_T v_P\cos\omega t\right) \\ &= v_P^2\left(\frac{v_T^2}{v_P^2} + \frac{v_P^2}{v_P^2} + 2\frac{v_T}{v_P}\frac{v_P}{v_P}\cos\omega t\right) \end{aligned} \tag{2.15}$$

$$= v_P^2\left(K_2^2+1+2K_2\cos 2\Phi\right)$$

It is now important to introduce the trigonometric relation

$$\cos 2\Phi = 1-2\sin^2\Phi \tag{2.16}$$

Introducing this expression into Eq. (2.15) yields

$$\begin{aligned} v_P^2\left(K_2^2+1+2K_2\cos 2\Phi\right) &= v_P^2\left[K_2^2+1+2K_2\left(1-\sin^2\Phi\right)\right] \\ &= v_P^2\left[\left(K_2^2+2K_2+1\right)-4K_2\sin^2\Phi\right] \\ &= v_P^2\left[\left(K_2+1\right)^2-4K_2\sin^2\Phi\right] \end{aligned} \tag{2.17}$$

and multiplying the expression on the righthand side of the equal sign by $(K_2 + 1)^2/(K_2 + 1)^2$, which is unity, to produce

$$v_P^2\left(K_2^2+1+2K_2\cos 2\Phi\right) = v_P^2\left(K_2+1\right)^2\left[1-\frac{4K_2}{\left(K_2+1\right)^2}\sin^2\Phi\right] \tag{2.18}$$

Thus, by substituting Eq. (2.18) into (2.15), (2.15) into (2.14), and (2.12) into (2.10), the arc length integral expression takes the form

$$\begin{aligned} S &= \int_0^{\Phi_1}\sqrt{v_P^2\left(K_2+1\right)^2\left[1-\frac{4K_2}{\left(K_2+1\right)^2}\sin^2\Phi\right]}\left(\frac{D}{v_P}d\Phi\right) \\ &= D\left(K_2+1\right)\int_0^{\Phi_1}\sqrt{1-\left[\frac{4K_2}{\left(K_2+1\right)^2}\right]\sin^2\Phi}\;d\Phi \\ &= D\left(K_2+1\right)\int_0^{\Phi_1}\sqrt{1-k^2\sin^2\Phi}\;d\Phi \end{aligned} \tag{2.19}$$

where,

$$k = 2\sqrt{K_2}/\left(K_2+1\right) \tag{2.20}$$

and

$$\phi_1 = \frac{\omega}{2} t_1 = \frac{1}{2}\cos^{-1}(1-2K_1) \tag{2.21}$$

Equation (2.19) represents an elliptic integral of the second kind, and solution tables of the integral for various values of ϕ_1 and k are readily available (Beyer, 1981).

It should be noted that τ and t_1 are different values:

(a) When $\tau > t_1$, it implies that the cutting of one chip is completed before the initiation of the next chip-cutting process.

(b) When $\tau = t_1$, it means that only one chip is being removed at a time.

(c) When $\tau < t_1$, it implies more than one chipping process exists at the same time.

Consequently, if the first grit produces failure according to the material failure criterion (e.g., Coulomb-Mohr for hard rock material such as granite) within the entire region enclosed by the two successive grits, then optimal use of the grits requires the grit spacing to be such that one chip is removed at a time (i.e., $\tau = t_1$).

Since the first and second chip curves are parallel and are offset by a distance, δ, the chip area can be found by summing all n^* of the differential area elements, $\delta\Delta h_k$, from the machined surface to the top of the workpiece surface (see Figure 2.3). This is mathematically expressed as:

$$A_c = \lim_{\Delta h_k \to 0} \sum_{k=1}^{n^*} \delta \Delta h_k = \delta h \tag{2.22}$$

This area can also be very accurately approximated[1] as the product of the curve length S and the mean chip thickness t_c

$$A_c \approx St_c \tag{2.23}$$

The next equation is used to equate the chip cross sectional area A_c relations

$$\begin{aligned} A_c\,(Eqn.\ 22) &= A_c\,(Eqn.\ 23) \\ \delta h &= St_c \end{aligned} \tag{2.24}$$

so that t_c can be solved, as shown

$$t_c = \frac{\delta h}{S} \tag{2.25}$$

Now, substituting the appropriate terms in this equation gives

$$t_c = \frac{K_2 \lambda h}{D(1+K_2)\int_0^{\phi_1} \sqrt{1-k^2 \sin^2 \Phi}\, d\Phi} \tag{2.26}$$

and since $K_1 = h/D$ and if divided by λ, a non-dimensional equation is formed

$$\frac{t_c}{\lambda} = \frac{K_1 K_2}{(1+K_2)}\left[\int_0^{\phi_1} \sqrt{1-k^2 \sin^2 \Phi}\, d\Phi\right]^{-1} \tag{2.27}$$

where, t_c/λ is called the *mean chip thickness to grit spacing ratio* or simply the thickness-spacing ratio.

---

[1]Note: In actuality our computation of S and A_c is still an approximation because we do not use the distance, δ, in computing the chip arc length, S. A better computation of A_c would consist of the average, S_{ave}, which would be derived from taking the average of the first grit's arc length, S, and the second grit's arc length, $\delta + S$.

$$S_{ave} = \frac{S+(\delta+S)}{2} = S + \frac{\delta}{2}$$

But since $v_T << v_P$ in most cases, δ is negligible in comparison to S. So, $S_{ave} \approx S$.

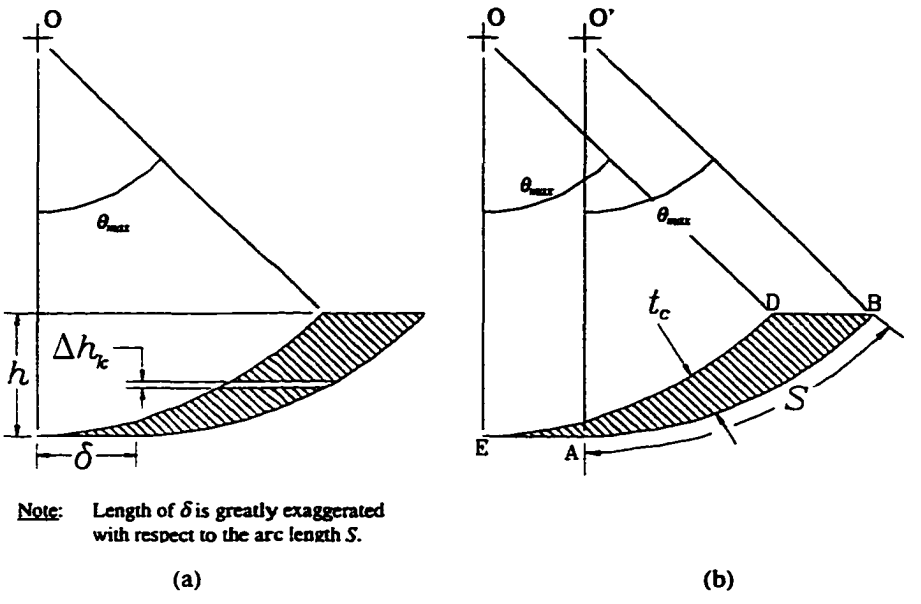

Figure 2.3 Methods of Determining Chip Cross Sectional Area. Figure (a) is a pictorial description of a theoretical chip which focuses on the differential area elements $\delta\Delta h_k$ used to calculate the chip cross sectional area, A_c. Figure (b) is an illustration of the same theoretical chip, but it focuses on the curve length, S, and the mean chip thickness, t_c. (Refer to Eqs. (2.22), (2.23), and (2.24) for details).

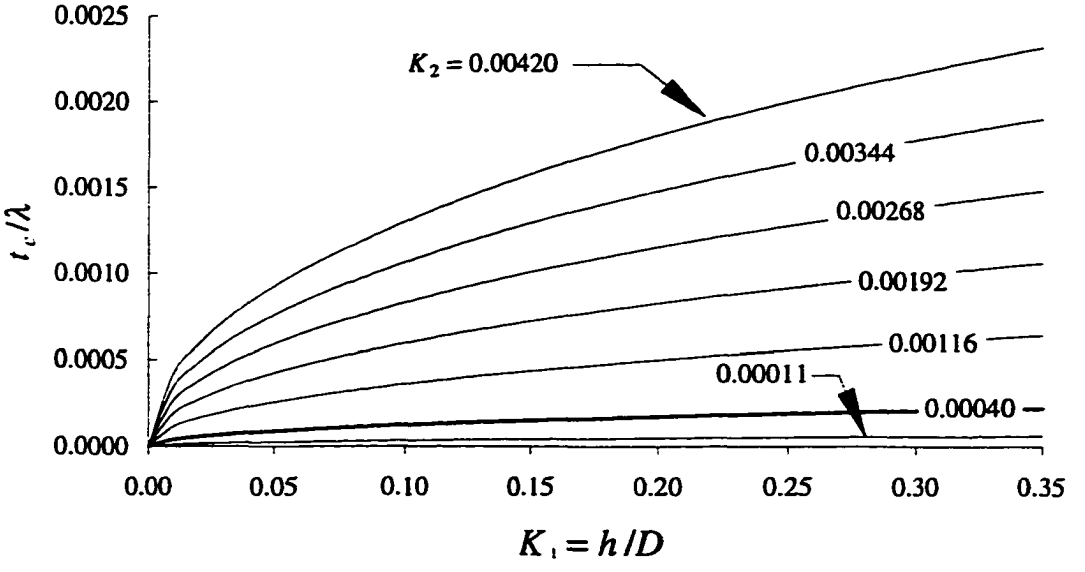

Figure 2.4 Non-Dimensional Chip Thickness of New Model.

2.4 Effects of Parameter Variation on Chip Thickness

Since a mathematical expression of the chip profile has been obtained in terms of the ratios' machining parameters, $K_1(h,D)$ and $K_2(v_T,v_P)$, their effect on the thickness-spacing ratio t_c/λ can now be examined. Since this ratio is a function of only two variables, K_1 and K_2, a two-dimensional graph has been produced which combines all of the relevant kinematics information (see Figure 2.4).

This graph encompasses the full range of practical machining ratios, K_1 and K_2. A depth-diameter ratio is the abscissa of the graph with a range of 0.0 to 0.35, and the speed ratio value was held constant for the computation of a single t_c/λ curve. The speed ratios vary from 0.00011 to 0.00420. Values of transverse rates as low as 0.3 m/min (1 fpm) have been reported (Bailey and Bullen, 1979; Bailey and Collins, 1977), and rates as high as 12 m/min have been recommended for multi-disc cutters (IMEX International, 1993). However, most literature shows that experiments are performed near the mid to lower end of this range (Pai, 1987; Ertingshausen, 1985). So the plotted range of K_2 is valid for transverse rates of approximately 0.3 to 5 m/min (1 to 16.4 fpm). Secondly, the plotted range of K_2 is valid for peripheral speeds, v_P, varying from 20 to 45 m/s (Ertingshausen, 1985; IMEX International, 1993).

The tool manufacturer denoted above lists the recommended maximum cutting depth h_{max} for each respective blade diameter, D. The ratio of these values (i.e., $K_{1max} = h_{max}/D$) shows a fairly linear variation from 0.20 to 0.35 for the entire range of blade diameters (200 to 3000 mm). Thus, the plotted range of K_1 values encompasses the lower ($K_1 \approx 0.0$), as well as the upper ($K_1 = 0.35$), limits.

Before discussing the trend of the plotted t_c/λ curve, the relationship of t_c with λ will be mentioned. The λ parameter is linearly proportional to the mean chip thickness, t_c. Physically, this means that as the distance separating each successive grit increases, the time required for the initiation of the second grit path likewise increases, according to Eq. (2.5). Hence, a larger chip will be produced. It should also be noted that this factor is a function of the diamond particle size, its concentration within the matrix material, and the parameter λ_{ss} (or β_s). λ_{ss} is defined as the ratio of the diamond segment length, L_{seg}, to the segment pitch, L_p, and β_s is defined as the ratio of the slot length, L_{slot}, to the segment length, L_{seg}. The λ_{ss} parameter, which is seen in some literature, is called the segment spacing ratio (Tönshoff and Warnecke, 1982). The β_s parameter is called the slot factor. These two parameters are related to each other by

$$\lambda_{ss} = \frac{1}{\beta_s + 1} \tag{2.28}$$

Intuition reveals that as the concentration increases, the number of active cutting grits should increase, thereby lowering the grit spacing factor λ and chip thickness t_c.

In actuality, only a fraction of the grits exposed to the surface are in contact with the workpiece, and hence do the cutting work (Löns, 1970; Wright and Wapler, 1986; Konstanty, 1991). This is because that the cutting edges are not all located at the same height, but are statistically distributed (Tönshoff and Warnecke, 1982). Thus, if some of the exposed diamonds make no contact with the workpiece, then it is obvious that of those diamonds which do make contact, only a fractional part of the grit diameter, is in contact with the workpiece (Büttner, 1974). Therefore, the surface density parameter C must be modified to account for these effects. In the study performed by Wright and Wapler

(1986), the lives of several grits exposed on the cutting surface of the diamond segment were followed. The life of each grit consisted of the time of initial exposure to the surface until its complete removal from the metal matrix binder. The grits used in their experiment had a 40/50 US Mesh size (average diameter of 400 mm) at a 30 concentration (0.264 gm/cm^3). It was found that approximately one-fourth (~25%) of the exposed diamonds make contact with the workpiece and actually perform the cutting operation. It was also found, once a reference datum for the matrix surface was set, that the working height of the particles consisted of those particles with at least 100 mm of diamond exposed to the surface. In summary, all of the above factors must be considered when analytically or numerically determining C or λ.

The t_c/λ curves, when plotted against K_1, all tend to have a positive non-constant slope. Each curve plotted is for a constant K_2 value. As the depth-diameter ratio increases ($K_1 > 0.10$), it is evident that the t_c/λ becomes fairly linear (i.e., constant slope). Reason implies that as the depth of cut is increased, more material must be removed, and in turn the chip thickness should also increase. The curve also shows that the diameter D varies inversely with t_c, and a larger diameter will lower the magnitude of τ. Consequently, δ will be smaller and thus, the chip thickness will be reduced. As a result, increasing the blade diameter while holding h constant (i.e., lowering K_1) will produce lower cutting force since less material will have to be removed.

The effect of the speed ratio, K_2, on t_c/λ is also apparent in Figure 2.4. The different curves for constant K_2 are equally spaced on the graph, and they tend to increase uniformly as K_2 increases. Increasing v_T will increase δ, and thus, the t_c will be increased. This means more material must be removed by the grit; thus, the chip

thickness t_c will be larger than at greater speed ratios. Therefore, it is safe to say that v_T is proportional to t_c, and v_P is inversely proportional to t_c. So, as the peripheral speed, v_P, is increased, the t_c value will be lowered. Physically, this trend is reasonable because v_P is inversely proportional to τ and δ. So, as v_P increases, the grit time lag, τ, which determines the length of δ, decreases. Thus, the chip horizontal offset is lowered, and the chip area and thickness are reduced.

2.5 Review of Previous Models

In previous single-point cutting theories, the shape of the chip cut in the grinding (or sawing) operation was considered to be a long, slender triangle (see Figure 2.5). Furthermore, the undeformed chip length l_c was considered to be approximately equal to the chord length AB since the contact angle θ_{max} was considered to be small (see Figure 2.3). Based on these approximations, a chip length of

$$l_c = \sqrt{Dh} \tag{2.29}$$

can be derived. Furthermore, Backer et al. (1952) derived an expression for the maximum chip thickness, t_{max}, using the chip's assumed triangular geometry and chip length, l_c. This expression simplifies to

$$t_{max} = \frac{2v_T\lambda}{v_P}\sqrt{\left(\frac{h}{D}\right)-\left(\frac{h}{D}\right)^2} \tag{2.30}$$

Since they assumed $h/D << 1$, the second-order term was neglected and

$$t_{max} = \frac{2v_T\lambda}{v_P}\sqrt{\frac{h}{D}} \tag{2.31}$$

$$t_{max} = \overline{DG}$$

Figure 2.5 Slender Triangle Chip Approximation (ref., Backer et al, 1952)

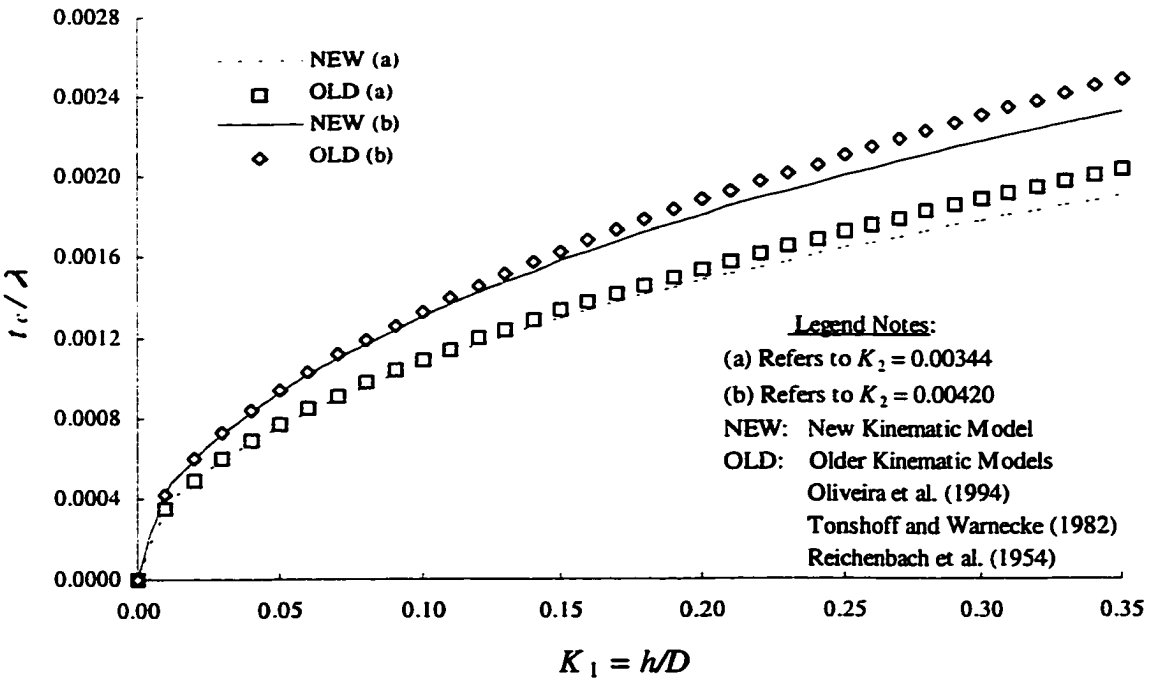

Figure 2.6 Non-Dimensional Chip Thickness Model Comparison

If the grit spacing, λ, is replaced by the terms

$$\lambda = \frac{1}{Cw_c} = \frac{1}{Cr(t_{max}/2)} \tag{2.32}$$

as given by Backer et al. (1952) and Pai (1987), then the well-known maximum chip thickness expression can be derived,

$$t_{max} = \sqrt{\frac{4v_T}{v_P Cr}\sqrt{\frac{h}{D}}} \tag{2.33}$$

as shown by Reichenbach et al. (1956), where C is the number of active cutting points per unit area on the blade (or segment) periphery; w_c is the average chip width; and r is the mean width to depth ratio of a scratch made by a single grit.

An alternate method for deriving the same expression for t_{max} can be obtained by using volume continuity. The volume of a single chip can be obtained in two ways: (a) by assuming the shape of the chip to be a long, slender triangle and (b) by dividing the material removal rate by the number of chips produced per unit time. By equating the relations developed in (a) and (b), an expression for t_{max} can be derived which is identical to Eq. (2.33) (Reichenbach et al, 1956; Shaw, 1979; Tönshoff and Warnecke, 1982).

Another chip parameter which many in this field have tended to use is the equivalent grinding thickness, t_{eq} ,

$$t_{eq} = \frac{v_T}{v_P} h = K_2 h \tag{2.34}$$

It can be considered as "...the sum of all instantaneous chip thicknesses in an arbitrary longitudinal section of the contact area" (Snoeys et al, 1974). But it has two drawbacks

in that "...it takes no account of the macro and microscopic structure of the cutting tool... [neither does it] ...provide comparable results when dealing with widely differing contact lengths," as noted by Tönshoff and Warnecke (1982). Oliveira et al (1994) have shown how the maximum chip thickness is related to the t_{eq} expression

$$t_{max} = \frac{2\lambda t_{eq}}{l_c} = \frac{2v_T\lambda}{v_P}\sqrt{\frac{h}{D}} \tag{2.35}$$

which is identical to Backer's expression in Eq. (2.31). Thus, although different approaches for deriving the t_{max} equation have been used by various researchers, their results simplify to the same expression.

2.6 Comparison with Proposed Model

To compare our model with those established by former researchers, the maximum chip thickness expression, Eq. (2.31) or (2.35), is rewritten in terms of the mean chip thickness. Since the shape of the chip was assumed to be in the form of a triangle, the mean chip thickness, t_c (or scratch depth), is simply one half the maximum chip thickness (i.e., 1/2 the height of the triangle). So, the mean chip thickness becomes

$$t_c = \frac{t_{max}}{2} = \frac{v_T\lambda}{v_P}\sqrt{\frac{h}{D}} \tag{2.36}$$

For the grinding operation it has been found experimentally that a good correlation exists between t_c and the resulting grinding forces and surface finish. This correlation was found to be a function of the speed ratio, K_2. Furthermore, the relationship was found to be linear when the t_c and the force and surface finish parameters were all plotted on logarithmic scales for constant values of K_2 (Snoeys et al, 1974).

It must also be remembered that the saw blade has a discontinuous cutting periphery consisting of diamond segments and air gaps (slots), whereas the grinding wheel has a continuous cutting periphery. Thus, another factor, the segment spacing ratio, λ_{ss}, must be included in the computation of the grit spacing, λ.

$$\lambda = f(C, r, t_c, \lambda_{ss}) \tag{2.37}$$

But the t_c expression given in Eq. (2.36), when divided by λ, produces an expression and curves for grinding models which are comparable to the sawing models.

$$\frac{t_c}{\lambda} = \frac{v_T}{v_P}\sqrt{\frac{h}{D}} = K_2\sqrt{K_1} \tag{2.38}$$

This expression can be attributed to all of the above mentioned researchers (Reichenbach et al, 1956; Tönshoff and Warnecke, 1982; Oliveira et al, 1994). The above expression has been plotted in Figure 2.6 along with the proposed model for two values for K_2, 0.00420 and 0.00344. The curves, t_c/λ, computed from Eq. (2.38) show excellent agreement with the proposed model. In the lower depth-diameter ratio range, $K_1 < 0.08$, the agreement is virtually perfect. This means the slender triangle assumption formerly used to compute t_c is verified or validated by the new model, whereas the mid to upper K_1 range (greater than 0.08) shows that our model predicts a chip thickness ratio value slightly less than the value in Eq. (2.38). At $K_1 = 0.20$ this difference is seen to be 3.9% for $K_2 = 0.00420$, and the difference gradually increases as K_1 increases. However, for a larger depth of cuts, the discrepancy reaches a maximum at the maximum allowable depth-diameter ratio. The primary reason for this difference is that a small angle approximation is used in the computation of the chip length, l_c, in the former models. This approximation begins to break down as the depth-diameter

ratio increases. This assumption is excellent for grinding operations where this ratio is usually very small. However, for sawing operations, the K_1 ratio is significantly larger. This difference can also be seen if the chip arc length to blade diameter ratio, l_c/D (or S/D), is plotted against the K_1 ratio (see Figure 2.7). And as with the t_c/λ curves, the l_c/D curve begins to deviate at $K_1 = 0.08$ from the exact arc length to diameter ratio S/D.

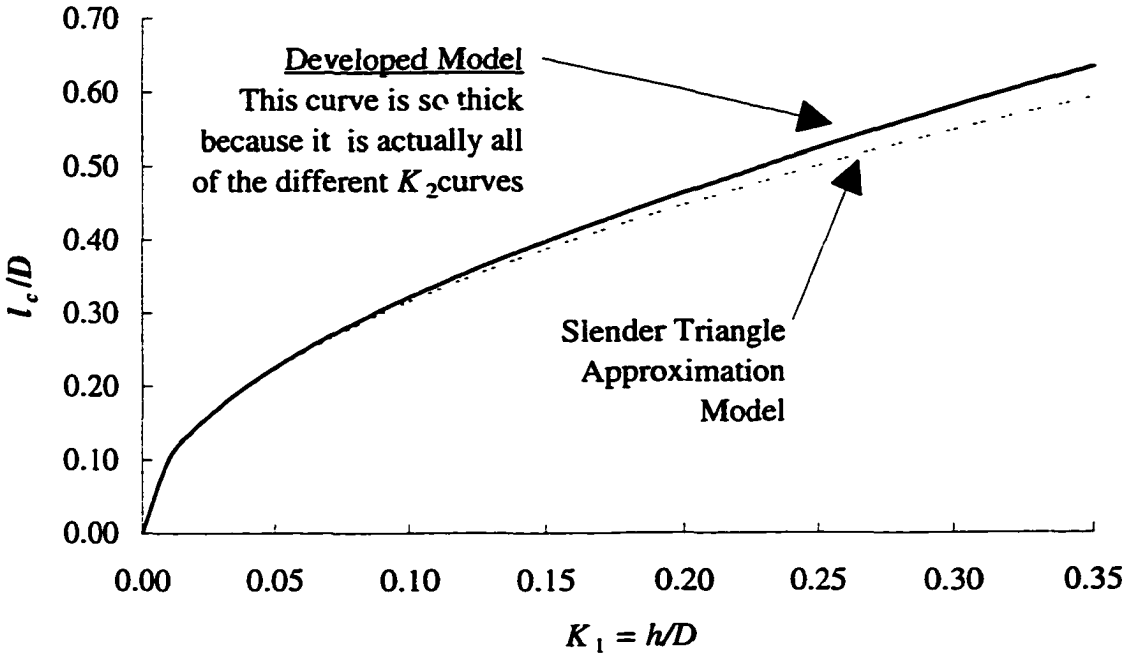

Figure 2.7 Non-Dimensional Chip Arc Length Model Comparison. See Appendix A for the table of l_c/D values which correspond to the above curves.

2.7 Cutting Force and Chip Thickness

A presentation of the new and old model has also been made on the graphs in Figures 2.8 and 2.9. They show the comparative cutting force plotted as a function of the chip thickness to grit spacing ratio. The data used in this graph is taken from old experiments performed by Burgess and Birle (1978) and Bailey and Bullen (1979). These curves exhibit a small degree of non-linearity, but for the most part both of them

are fairly linear (even on a non-logarithmic scale). This curve follows the usual trends of sawing, that is, the resultant cutting force, F_t, increases as the size of the chip thickness, t_c, increases (or t_c/λ increases). This occurs because more energy is required to remove larger chips. These curves illustrate that the chip thickness-spacing ratio, t_c/λ, for the new model is slightly smaller than for the old model, especially at the upper t_c/λ range. Since for the given case the F_t value has been experimentally determined, it possesses the same value for both models. Thus, if the cutting stresses were computed using both the old and new models, the new one would indicate higher stresses than the old model.

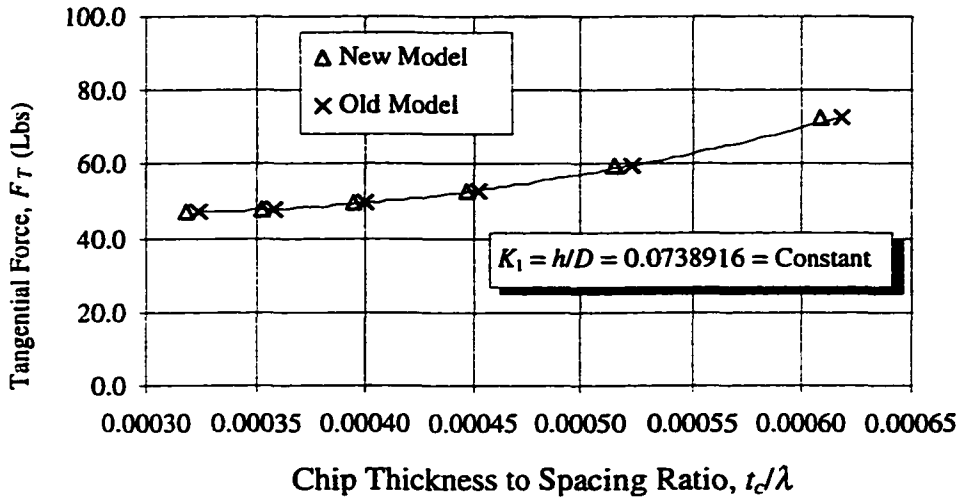

Figure 2.8 Cutting Force as a Function of Chip Thickness-Spacing Ratio (Experimental Data Taken From Burgess & Birle, 1978)

Practically, it should be the goal of every model to accurately and faithfully describe the physical phenomena it is characterizing, especially if the results of the model influence the results of another model that is dependent upon it. Accordingly, the new model is being used in conjunction with a recently developed 3-dimensional grit spacing λ model (see Jerro et al., 1997) to explicitly determine t_c.

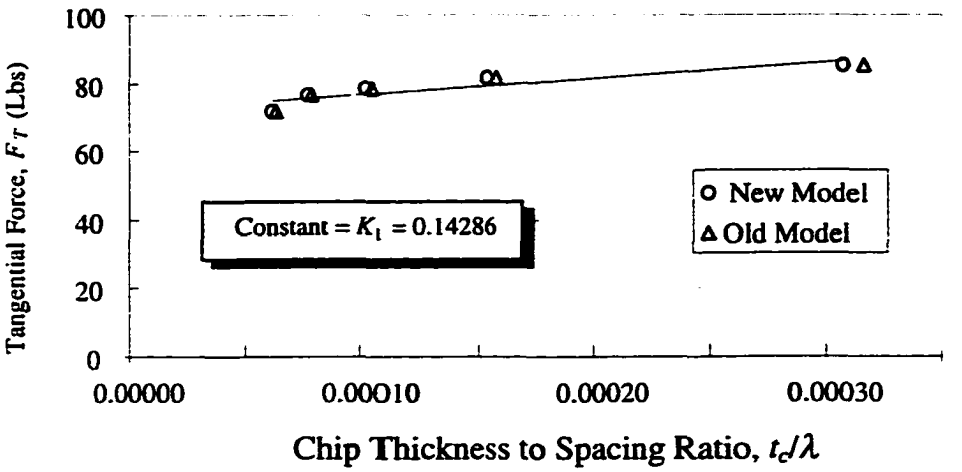

Figure 2.9 Cutting Force as a Function of Chip Thickness-Spacing Ratio (Experimental Data Taken From Bailey & Bullen, 1979)

In summary, therefore, the practical significance of the proposed model is twofold. First, the new model should be used for the sawing process, especially at relatively moderate to large K_1 values (i.e., greater than 0.08). Secondly, other parameters, such as grit cutting force models and grinding ratio G (the ratio of volume of cut material to the volume of tool wear), use the mean chip thickness, t_c, as an input parameter (Tönshoff and Warnecke, 1982; Oliveira et al, 1994). Therefore, by using t_c from the new model, these parameters' values will be modified and improved.

CHAPTER 3

GRIT DISTRIBUTION ANALYSIS

3.1 Analysis Objectives

It is known that the value of λ is influenced by independent diamond tool properties, such as grit concentration and size, segment dimensions, etc. In the grinding process, from which many diamond tool sawing relations and analogies have been drawn, it has been shown that λ is influenced by the dynamic machining parameters (Brecker and Shaw, 1974). However, in normal grinding processes (such as surface grinding) there are far more abrasive particles (grits) present than in typical diamond tool sawing. Secondly, even though most of the grinding bonds are hard, they can be flexible, whereas, the metallic bond used for the diamond saw is more rigid. Therefore, the grit spacing under the static and dynamic cases should be the same (Boothroyd and Knight, 1989). So in this paper the study will be limited to static conditions.

Thus, the objective will be determining grit spacing as a function of only the independent tool properties mentioned above. To accomplish this task, a two fold modeling approach will be used:

(1) In the first approach an analytical model is developed to characterize the distribution of grits in a uniform way. From the periodicity which arises in uniformity, a value for the grit spacing term λ can be computed.

(2) In actuality because of the mixing of grits and matrix powders, the positioning of the grits in the matrix is far from uniform, but instead is very random. To take the effects of randomness into account, a numerical model and "brute force" computer algorithm has been developed. This algorithm models the random characteristics of the segment surface and grit positioning and then computes the grit spacing, λ, based on these characteristics.

To ensure the validity of our analytical and numerical models, they are compared for several typical sawing cases. With a definite knowledge of λ, the response of other important parameters can be inferred, such as cutting force and power. Also, if the t_c/λ ratio is known as given in Eq. (2.27), then explicit computation of t_c will also be possible. This is important because it is well known that the chip thickness, t_c, is proportional to the relative chip cutting force.

3.2 Review of the Surface Density Parameter

The typical size of the synthetic diamond grits used in the circular sawing of stone and concrete generally ranges between 150 and 900 μm. Thus, trying to count these particles with the naked eye is very impractical. Instead, one relies on the light microscope for segment surface information or the scanning electron microscope (SEM) for even more detailed surface characterization (Tönshoff and Warnecke, 1982; Tönshoff and Schulze, 1982; Liao and Luo, 1992; Mirshams, Crosby, and Thomas, 1994).

The surface density parameter C (i.e., number of grits per unit surface area, sometimes designated as N_D) has been predominately used in the past for grinding as well as sawing instead of the grit spacing, λ (Brecker and Shaw, 1974). In fact, most of the

former chip thickness equations are formulated under the assumption that this parameter, C, can be experimentally determined (Büttner, 1974; Tönshoff and Warnecke, 1982). For example, one study reported finding a total in excess of 400 grits when six segments were examined on a 350 mm blade (Bailey & Bullen, 1979). This means the cutting face of each segment should have possessed an average of approximately 70 grits. The parameter C could then be found by simply dividing the number of grits observed on the surface by the surface area of the segment, as shown in the following equation

$$C = \frac{No.\,of\ observed\ grits}{segment\ surface\ area} \tag{3.1}$$

In another work Brecker and Shaw (1974) developed an experimental method to measure C during the cutting operation (i.e., dynamically) of a grinding wheel. Vibration and elastic deflection effects are included in dynamic grinding measurements. In their work they also counted the number of oscilloscope blips to determine the number of cutting points, N, and used the equation

$$C = \frac{N}{\tau v_p b} \tag{3.2}$$

where τ is the grinding time and b is width of the razor blade. As mentioned earlier, they found C to be a function of the machine parameters (h, D, v_p, and v_T). They also noted other researchers who used various techniques to measure C, such as Peklenik (1957), who used an imbedded thermocouple technique to measure linear grit spacing, and Backer et al. (1952), who used a dressed grinding wheel on a soot-covered glass surface to obtain the average number of grains per unit area.

A quick estimate of the surface density, C, can be analytically determined by using the known tool parameters of grit size, d_g (i.e., average grit diameter), and the density of diamond, ρ, concentration of grits in matrix, C^*. The concentration, C^*, is the diamond industry trade name for the mass-to-volume ratio of diamond grits in the segment. It must be used in conjunction with (i.e., multiplied by) the factor α_c so that the actual mass per unit volume (gm/cm^3) of grits in the segment can be obtained. The value of α_c is 0.0088 gm/cm^3. These parameters can be used to compute the total number of grits, N_{DT}, contained in a single segment, which is given by the equation

$$N_{DT} = \frac{V_{Tg}}{V_{1g}} = \frac{m_{Tg}/\rho}{V_{1g}} \tag{3.3}$$

where,

m_{Tg} = total mass of grits in segment = $V_{seg}\ \alpha_c C^*$

V_{Tg} = total volume of grits in segment = m_{Tg}/ρ

V_{1g} = volume of one grit = $\pi d_g^3/6$

V_{seg} = volume of segment = $L_{seg} W_{seg} H_{seg}$

L_{seg} = segment length

W_{seg} = segment width

H_{seg} = segment height at fabrication.

Since the grits are randomly distributed, a graph is used to illustrate the cumulative distribution of grits in the segment (see Figure 3.1). The cumulative number of grits in the segment N_{DC} is given as a function of z, the distance from the base of the segment, $z = 0$, to any position, $z = a$. This number can be written first using the integral formulation as

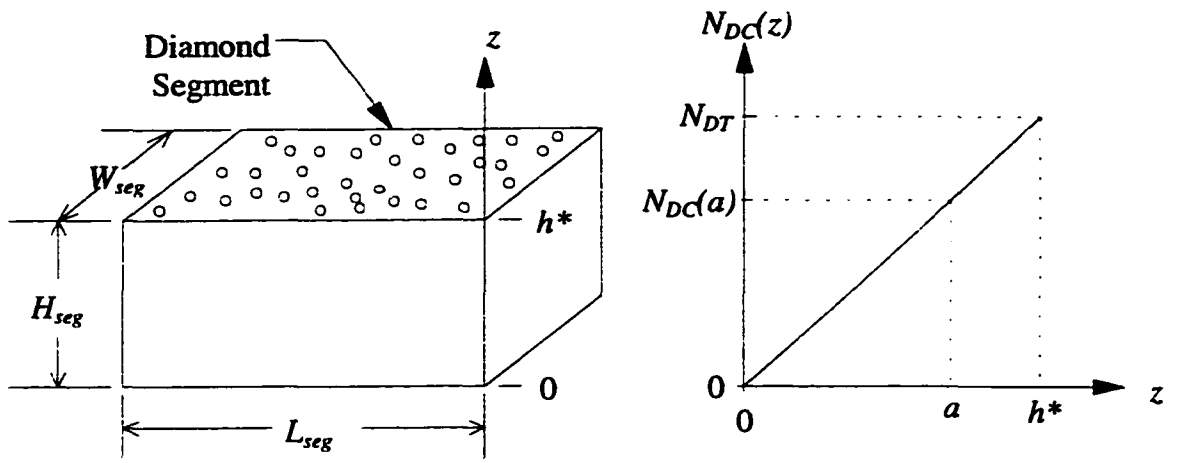

Figure 3.1. Illustration of Diamond Composite Segment and Cumulative Grit Distribution Curve.

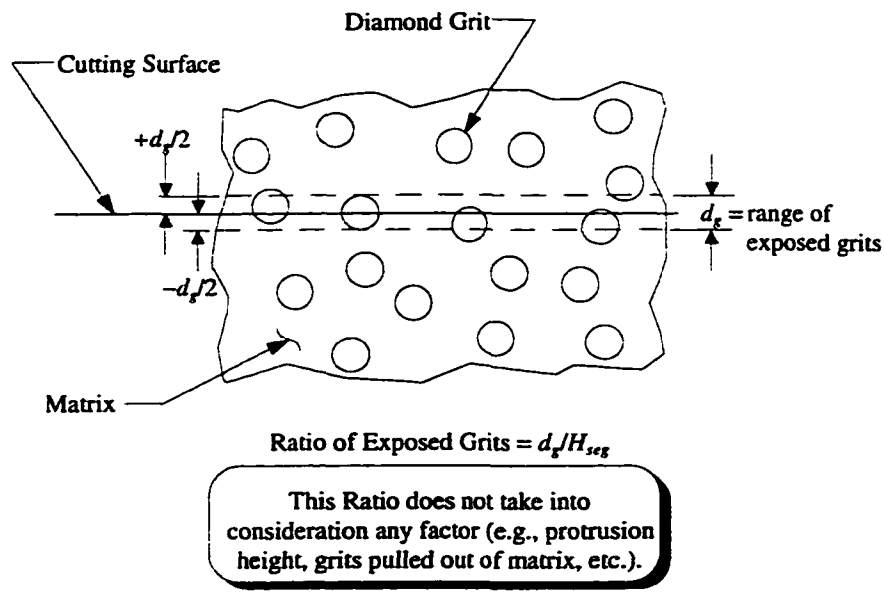

Figure 3.2. Illustration of Range of Exposed Grits

$$N_{DC}(z) = \int_0^z N'_D(z')dz' \tag{3.4}$$

where N'_D equals the slope of the $N_{DC}(z)$ line. Because of the random nature of the particle distribution, N'_D should vary from point to point along the z-axis. But because of the large number of particles, N'_D should possess a fairly constant value (or average) which can be used in subsequent computations. So

$$N_{DC}(z) = N'_D z \tag{3.5}$$

At $z = z_{max} = H_{seg}$, $N_{DC}(H_{seg})$ equals the total number of grits in the segment, N_{DT}, or

$$N_{DT} = N_{DC}(H_{seg}) = N'_D H_{seg} \tag{3.6}$$

Since N_{DT} can be readily computed, as shown in Eq. (3.3), and $z_{max} = H_{seg}$ is known, N'_D can be determined

$$N'_D = \frac{N_{DT}}{H_{seg}} \tag{3.7}$$

But since the grit surface density is sought, the total number of grits exposed, N_{DE}, at any location, z (without making any differentiation to protrusion height, grits pulled out of the matrix, or any other factor), is required. This quantity, N_{DE}, is found by including all of the grits which have their centers within the grit diameter range d_g of the cut surface, as shown in Figure 3.2. N_{DE} is computed by multiplying the slope term N'_D by d_g as shown below

$$N_{DE} = N'_D d_g = N_{DT}\left(\frac{d_g}{H_{seg}}\right) \tag{3.8}$$

where the ratio of exposed grits at any location, z, without regard to any factor, is d_g/H_{seg}. Therefore, the grit surface density can be computed

$$C = \frac{N_{DE}}{W_{seg} L_{seg}} = \frac{N'_D d_g}{W_{seg} L_{seg}} \tag{3.9}$$

and, after a little algebraic manipulation,

$$C = \frac{6\alpha_c C^*}{\pi \rho d_g^2} \tag{3.10}$$

However, it must be remembered that this equation yields a *high estimate* of the surface density.

Research has found that in actuality only a fraction of the grits exposed to the surface are in contact with the workpiece and, hence, do the cutting work (Löns, 1970; Wright and Wapler, 1986; Konstanty, 1991; Liao et al., 1997). This is because that the cutting edges are not all located at the same height, but are statistically distributed (Tönshoff and Warnecke, 1982). Thus, if some of the exposed diamonds make no contact with the workpiece, then it is obvious that of those diamonds which do make contact, only a fractional part of their grit diameter is in contact with the workpiece (Büttner, 1974). Therefore, the surface density parameter, C, must be modified to account for these effects. In the study performed by Wright and Wapler (1986) they followed the life of several grits exposed on the cutting surface of the diamond segment. The life of each grit consisted of the time of initial exposure to the surface until its complete removal from the metal matrix binder. The grits used in their experiment had a 40/50 US Mesh size (average diameter of 400 μm) at a 30 concentration value, C^*, of 30 (which is equivalent to 0.264 gm/cm^3). It was found that approximately one-fourth (25%) of the exposed diamonds make contact with the workpiece and actually perform the cutting operation. It was also found that once a reference datum for the matrix surface was set, the working height of the particles

consisted of those particles with at least 100 μm of diamond exposed to the surface. In summary, all of the above factors must be considered when analytically or numerically determining C or λ.

3.3 Segment Surface Model

Before discussing the analytical or numerical methods used to determine the grit spacing, the model used to characterize the segment surface is discussed. Since the diamond grits are generally rough, blocky, irregular spheres, it will be assumed for modeling purposes and simplicity that they take a perfectly spherical shape (Tönshoff and Warnecke, 1982; Jennings and Wright, 1989; Konstanty, 1991). The surface of the segment is characterized by fractured (or worn), polished, newly exposed grits and grit craters. Usually, fractured grits are those which have lost a portion of their protrusion height due to impact or wear. The exposed surface of the polished grits has been worn in such a manner as to render the grit dull and inefficient for cutting. Much information on these grits and the segment surface was also given in the previous section, such as facts about the percentage of working grits and fractional diameter contact. Research has also found that at least 60% of the grit must be retained by the matrix material (Büttner, 1974). This leaves only 40% of the volume of the grit exposed to the surface. Thus, when less than 60% of the grit is retained by the matrix, grit "pull-out" is highly probable. Grit "pull-out" occurs when the cutting force exceeds the matrix retention force and the grit is pulled out of its position in the matrix. In those instances a crater (or hole) is left on the segment surface in the matrix. For example, Figure 3.3 shows four grits on the exposed surface. Part (a) of the figure shows a three-dimensional (3-D) illustration of this arrangement, while (b) shows a side view. It is evident from (b) that, although Grit # 4

lies on the exposed plane of the matrix, it clearly would not be retained by the matrix because 70% of its volume is exposed to the surface, whereas, Grits # 1, # 2, and # 3 are all firmly retained by the matrix. Thus, at the location of Grit # 4, the actual surface as seen through a microscope would be a "crater." A couple of photomicrographs of these effects is given in Appendix B.

Since a specific amount of diamond grit must be retained by the matrix, only a fixed number of particles will be present on the surface. Secondly, if it is assumed that all of the exposed grits obey this retention model, then a reference datum can be established at this level (i.e., 60% grit retention), and the maximum protrusion height, Δr_{Pmax}, with respect to this datum would be known (see Figure 3.4). An equation to calculate this height has been derived using the geometry of the grit and the maximum percentage of the material exposed to the reference datum. The derivation of this equation begins by recalling the volume of one spherical grit:

$$V_{1_g} = \frac{\pi}{6} d_g^3 \tag{3.11}$$

The region of the grit above the reference datum (i.e., matrix surface) is called a spherical cone. The volume of this cone (V_{SC}) is given as

$$V_{SC} = \frac{\pi}{6} \Delta r_P^2 \left(3d_g - 2\Delta r_P\right) \tag{3.12}$$

where Δr_P is the protrusion height of the grit and is defined as the vertical distance from the reference datum to the top of the grit (see Figure 3.5) (Beyer, 1981). Thus, the volume percentage exposed (V_{PE}) to the cutting surface can be computed as the ratio of spherical cone volume to the grit volume,

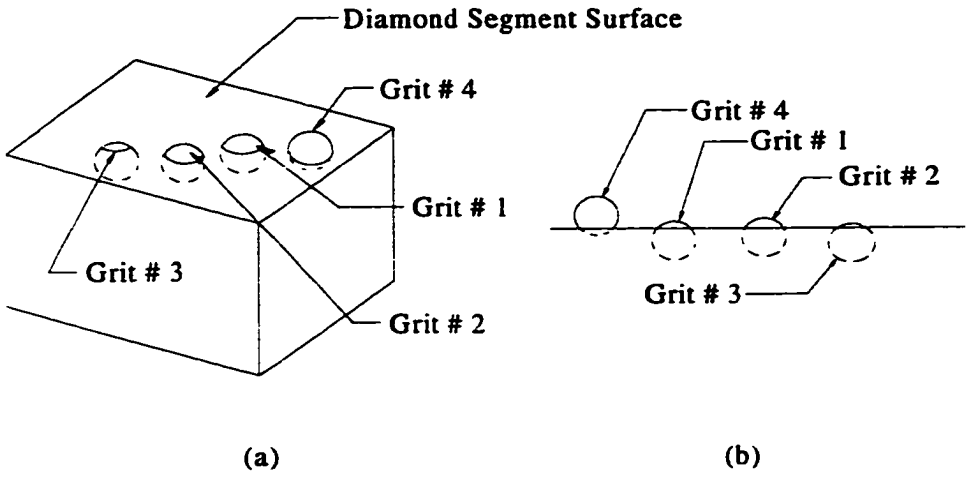

Figure 3.3. Grits on Exposed Diamond Segment Surface for Spherical Model

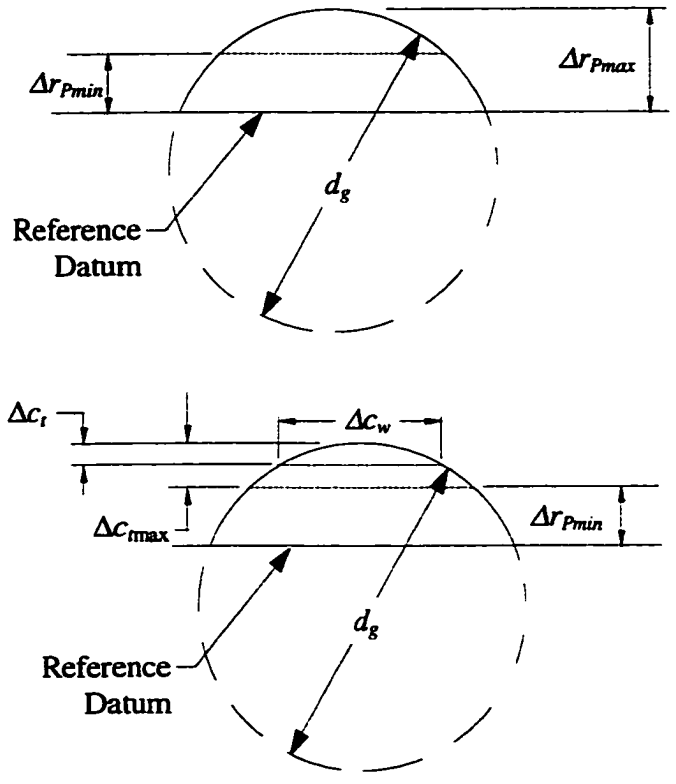

Figure 3.4. Maximum and Minimum Protrusion Heights of Exposed Diamonds

$$V_{PE} = \frac{V_{SC}}{V_{1g}} \times 100\% \tag{3.13}$$

Now inserting Eqs. (3.11) and (3.12) into Eq. (3.13) and rearranging the new equation yields a cubic equation in terms of Δr_P

$$2\Delta r_P^3 - 3d_g \Delta r_P^2 + \frac{V_{PE} d_g^3}{100} = 0 \tag{3.14}$$

The solution for Δr_P in this equation represents the maximum protrusion height, Δr_{Pmax}, of the grit in the matrix before pull out occurs. Out of three possible solutions for Δr_{Pmax}, only one is valid for the geometric constraints of the problem. This solution is given as

$$\Delta r_{P\max} = \left\{ \frac{1}{2} + \cos\left[\frac{1}{3} \cos^{-1}\left(1 - \frac{V_{PE}}{50} \right) + \frac{4\pi}{3} \right] \right\} d_g \tag{3.15}$$

where V_{PE} is the maximum volume percent of grit exposed to the cutting surface. Furthermore, only a fraction of these exposed grits are at the correct height to be in contact with the workpiece. Because of the statistical distribution of the heights of the surface grits, it has been shown that the cumulative relative protrusion height, $\Delta r_P/\Delta r_{Pmax}$, corresponds in a nearly linear manner to the relative number of surface grits, N/N_{max}, (Tönshoff and Warnecke, 1982). For example, if 25% of the surface grits are at the working height, then their corresponding heights are represented by the upper limits of the relative protrusion heights (i.e., $\Delta r_P / \Delta r_{Pmax}$ from 0.75 to 1.0). Based on this model, an equation for the minimum working height, Δr_{Pmin}, has been developed and is given as

$$\Delta r_{P\min} = \left(1 - \frac{P_{WH}}{100} \right) \Delta r_{P\max} \tag{3.16}$$

where P_{WH} represents the percentage of grits making contact with the workpiece surface. Therefore, the maximum grit thickness of cut, Δc_{tmax}, can be determined from the above constraints,

$$\Delta c_{t\max} = \Delta r_{P\max} - \Delta r_{P\min} \tag{3.17}$$

This thickness of cut is exact for only the grit(s) exhibiting maximum protrusion, but because of the normal distribution of the working grits, the average cut thickness, Δc_t should be one half of this value

$$\Delta c_t = \frac{\Delta c_{t\max}}{2} \tag{3.18}$$

From the average thickness of cut and geometry of the grit, an average width of cut Δc_w can be computed,

$$\Delta c_w = 2\sqrt{\left(d_g - \Delta c_t\right)\Delta c_t} \tag{3.19}$$

This width of cut is also referred to as the average working height diameter, d_{wh}. The importance of Δc_{tmax} and Δc_w will be evident in forthcoming sections of this paper.

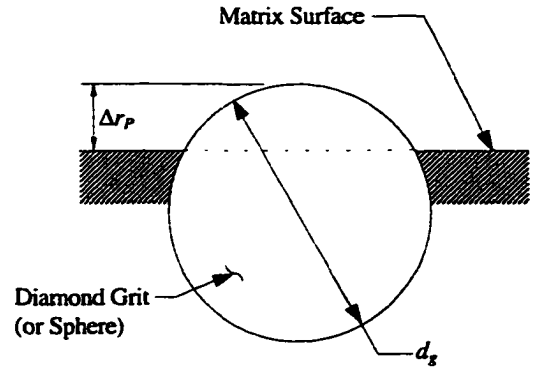

Figure 3.5 Protrusion height (Δr_P) of exposed diamond

3.4 Analytical Model

3.4.1 Particle Distribution Transformation

As mentioned earlier, the mixing of the grits and metal matrix material is carried out in such a way that the particles are randomly distributed throughout the matrix. This means that the large number of particles (on the order of 10^3 to 10^4) should be uniformly distributed. However, the particles do not sit in uniformly spaced positions throughout the matrix, but rather at random points in 3-D space, and this makes determining the spacing or periodicity of the cutting grit very difficult.

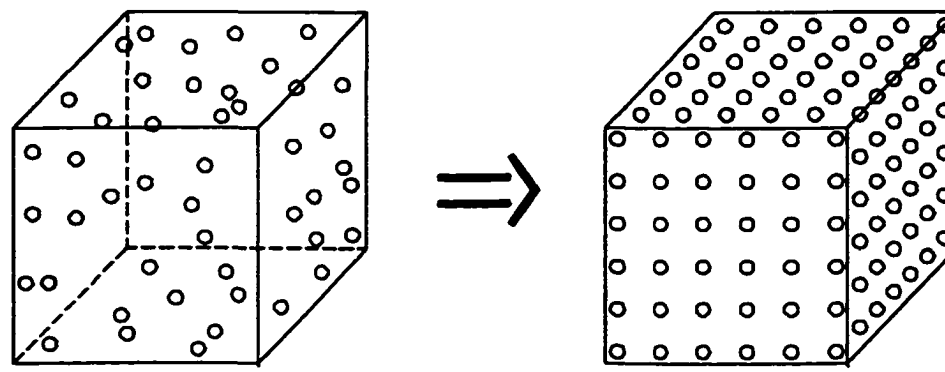

Random Particle Distribution

Uniform Particle Distribution

Figure 3.6 Illustration of Particle Distribution Transformation.

It is postulated that a volume of randomly distributed particles can be equivalently (or geometrically) viewed as a volume of uniformly spaced particles. This means transforming one particle arrangement into another as shown in Figure 3.6, and this is made possible because the density of particles is a known and controllable property. Thus, equivalent sawing mechanics will occur with the uniform arrangement that occurs with the actual random arrangement. This argument leads to the mentioning of the two important

factors that need defining: (1) the unit particle volume, *UPV*, and (2) the *UPV* arrangement factor. However, before the *UPV* can be determined, the effective particle density must be known.

3.4.2 Effective Particle Density

In the typical grinding operation, the abrasive and matrix material is continuous along the periphery of the grinding wheel. However, the circular diamond saw is constructed with a discontinuous periphery. The discontinuity arises from the use of slots at equally spaced locations between the segments along the periphery (see Figure 2.1). There are several benefits resulting from the addition of these slots, such as debris removal and coolant flow enhancement (Yang et al., 1994). The particle density of the segment and one adjacent slot is now calculated. This density is defined as the number of particles which occupy one unit volume of the matrix. If the segment volume is placed beside its adjacent slot volume, the density of the diamond grits (particles) of the total volume (the union of the segment and slot volumes) can be found (see Figure 3.7). First, the particle density of the segment γ_{seg} is given as

$$\gamma_{seg} = \frac{N_{DT}}{V_{seg}} = \frac{N_{DT}}{L_{seg} H_{seg} W_{seg}} \tag{3.20}$$

Secondly, the particle density of the slot, γ_{slot}, is known to be zero. However, the particle density of the entire volume, γ_p, is the total number of particles divided by the total volume,

$$\gamma_p = \frac{N_{DT}}{V_{seg} + V_{slot}} = \frac{N_{DT}}{(L_{seg} + L_{slot}) H_{seg} W_{seg}} \tag{3.21}$$

where V_{slot} and L_{slot} are defined as the volume and length of slot, respectively. Rearranging the above equation and dividing by L_{seg} yields

$$\gamma_p\left(1+\frac{L_{slot}}{L_{seg}}\right) = \frac{N_{DT}}{L_{seg}H_{seg}W_{seg}} = \gamma_{seg} \tag{3.22}$$

and

$$\gamma_p = \frac{\gamma_{seg}}{1+\beta_s} \tag{3.23}$$

where,

$$\beta_s = \frac{L_{slot}}{L_{seg}} \tag{3.24}$$

Physically, β_s is the ratio of the slot length to the segment length, as denoted in Chapter 2. It will be referred to simply as the "slot factor." The range of this factor varies from 0.075 to 1.25 when examining available disc sizes from a leading diamond tool manufacturer (IMEX International, Inc., 1993). Thus, including the slot factor β_s will decrease the particle density of the segment γ_p to 44 to 93% of its original value.

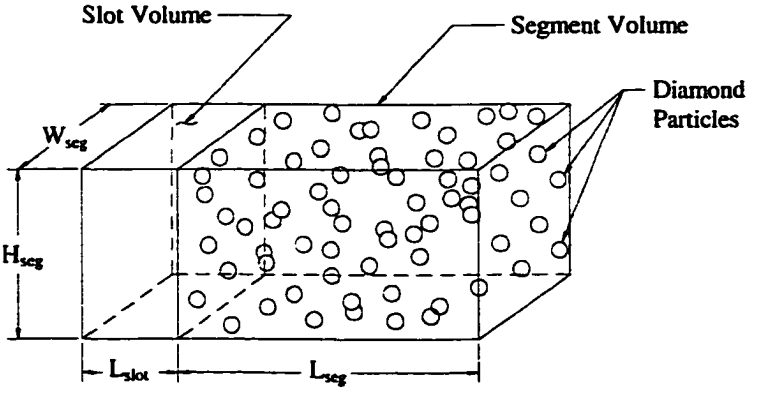

Figure 3.7 Union of the Segment and Slot Volumes.

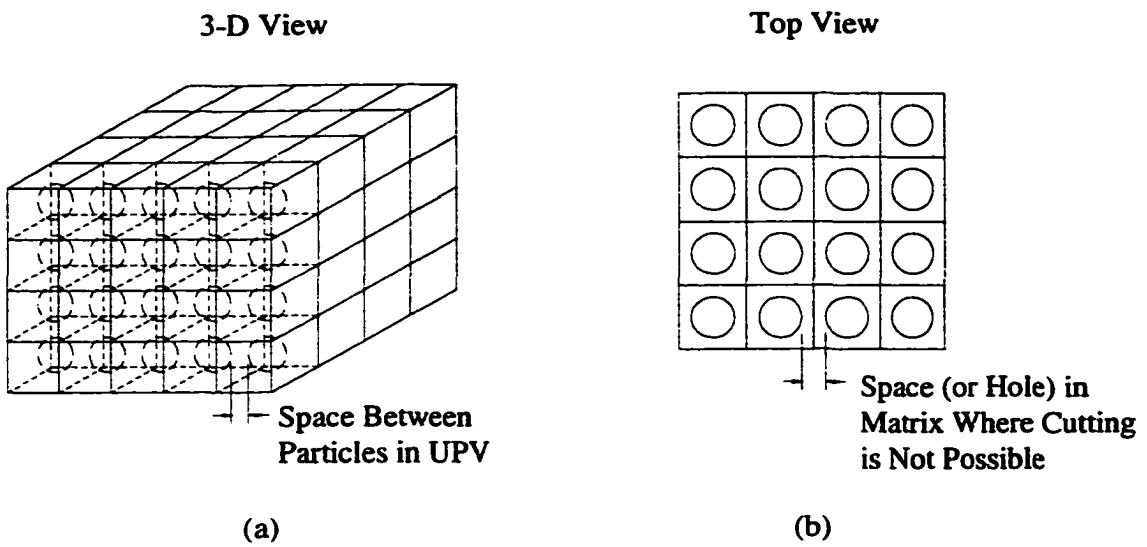

Figure 3.8 Cubic Array of Unit Particle Volumes.

3.4.3 Unit Particle Volume

The unit particle volume is more easily recognized as the inverse of the particle density. From the definition given above for particle density, intuition reveals that a unit particle volume represents the magnitude of the cubic volume which surrounds the particle. This volume also includes the volume of the particle. So the equation for the magnitude of the *UPV* is given as

$$UPV = L_{UPV}^3 = \frac{1}{\gamma_p} \tag{3.25}$$

where L_{UPV} is the side length of the *UPV*. One subtle feature of this parameter is that its magnitude is larger than that of the particle. So, if a large number of these volumes are stacked upon one another and side-by-side in building block fashion, the individual particles, encased in these volumes, would not touch one another as shown in Figure 3.8. Hence, no cutting could be performed in the matrix space where no grits lie. The leads to the introduction of the *UPV* arrangement factor.

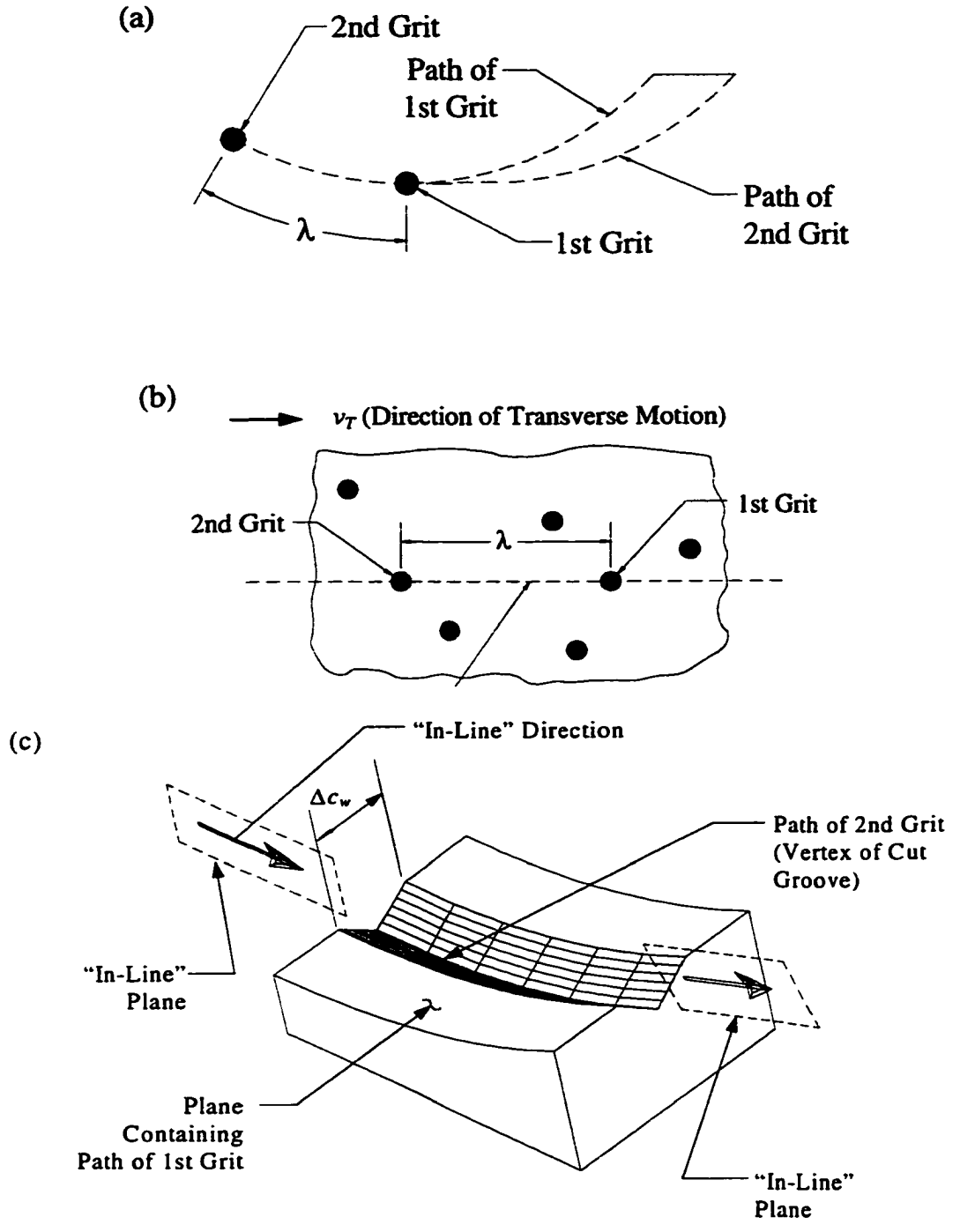

Figure 3.9. Illustrations of "In-Line" Plane and Direction

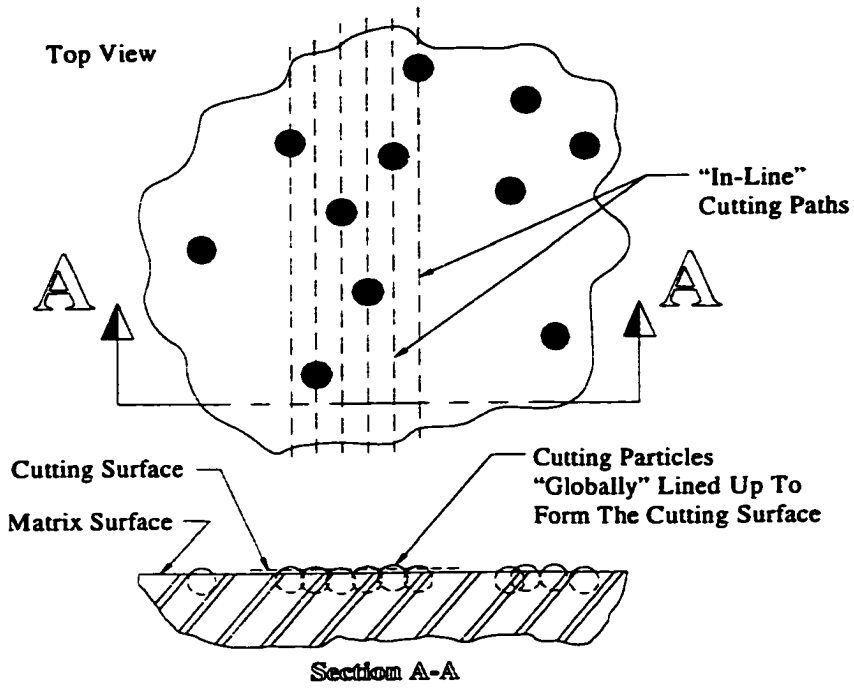

Figure 3.10. In-Line Cutting Path (A Global View)

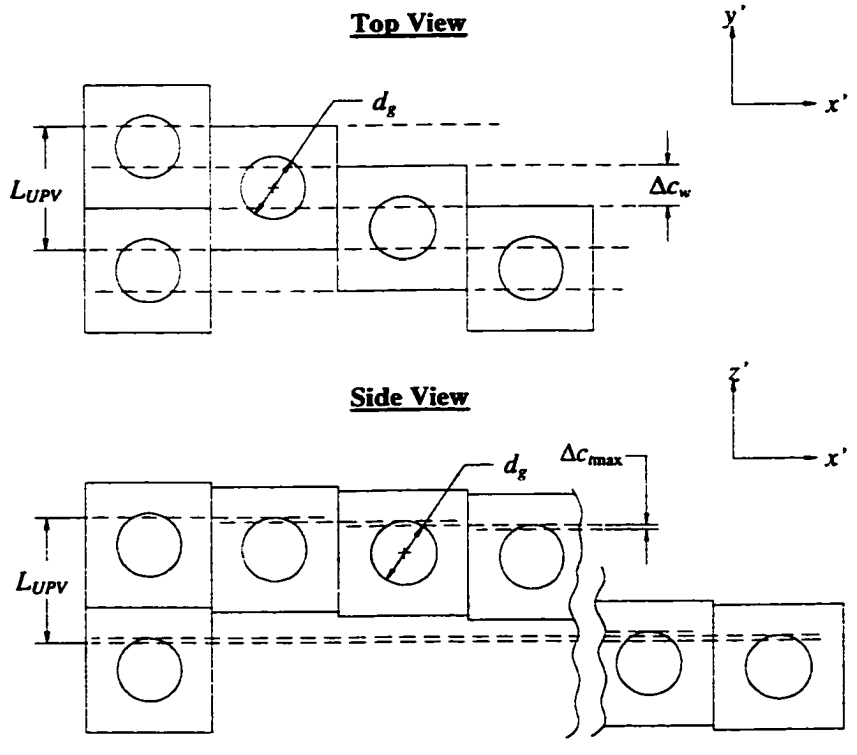

Figure 3.11. UPV Lateral and Vertical Offsets

3.4.4 Unit Particle Volume Arrangement Factor

Perhaps briefly reviewing the grit spacing, λ, (or "in-line" spacing) term would better give an understanding of the need and importance of the *UPV* arrangement factor. According to our cutting model, an individual grit on the periphery of the saw blade performs the actual cutting of the workpiece. The grit traces a cycloidal-type path into the workpiece. After this grit has completed its path, it is followed by a second grit, which traces out a secondary path into the workpiece (see Figure 3.9a). The area enclosed by these two paths forms what is known as a chip. Furthermore, the second grit will cut a chip if, and only if, it lies directly "in-line" with the first cutting grit. This is parallel with the direction of transverse motion. It is well understood that not all chips are cut with perfectly "in-line" grits when they are randomly distributed. They may be slightly or greatly off the "in-line" path. But for the purpose of modeling, the "in-line" approach is applicable because a uniform particle distribution approach is used. Figure 3.9b shows that the "in-line" grits are separated by λ. This parameter is defined as the grit "in-line" spacing distance. Figure 3.9c gives a 3-D illustration of the "in-line" direction and plane.

As mentioned earlier, the size of the *UPV* is larger than the diamond particle size. Thus, a standard 3-D array (see Figure 3.8) of *UPV*s would not allow the particles to touch. In other words, holes would be left in the matrix where cutting would not be possible. However, cutting would be possible if the *UPV*s were arranged (stacked) in such a way that the cutting portions (i.e., upper top sector) of the grits were lined up side by side laterally across the cutting surface. This side by side position does not have to occur locally but in a "global" sense as shown in Figure 3.10. Thus, the key to finding the "in-line" grit spacing, λ, is determining a stacking arrangement which will provide (1) the

periodicity which would be found in a uniform particle distribution and (2) the cutting surface that is developed when the particles are "globally" lined up side by side.

The main driving force behind the solution of the problem is ensuring that complete coverage on the cutting surface is achieved. This surface may be any imaginary horizontal plane within the segment. Thus, lateral as well as vertical cutting coverage must be completely achieved. This can be accomplished by offsetting each adjacent unit cell volume in the lateral (y') direction by the width of grit cut Δc_w and also offsetting each cell in the vertical (z') direction by the maximum thickness of cut Δc_{max}. The lateral offset is illustrated in the top view of Figure 3.11. It can be seen that after so many offsets are accomplished, repetition of the initial *UPV* is achieved. Thus, for the illustrated case, Figure 3.11, three offsets are required to achieve one cycle. A new parameter is now introduced, the lateral arrangement factor, k_{afl}, which is the number of offsets required for a complete *UPV* cycle. The value for this parameter may be found by dividing the side length of a *UPV* by the width of grit cut, that is

$$k_{afl} = \frac{L_{UPV}}{\Delta c_w} \tag{3.26}$$

This parameter may or may not be an integer, but this factor is unimportant. However, if k_{afl} is not an integer, a slight overlapping of the working path widths will occur. The vertical offset is illustrated in the side view of Figure 3.11. As noted earlier, this offset distance is defined as the maximum thickness of grit cut, Δc_{max}. And as with the lateral case, a vertical arrangement factor, k_{afv}, is required to quantify the number of offsets needed to achieve one *UPV* cycle. Hence, the equation for this factor is

$$k_{afv} = \frac{L_{UPV}}{\Delta c_{t\max}} \tag{3.27}$$

Now that the lateral and vertical arrangement factors have been defined, the transverse arrangement factor, k_{af}, can be determined. It is simply the product of the lateral and vertical factors, or

$$k_{af} = k_{afl} k_{afv} = \frac{L_{UPV}^2}{\Delta c_w \Delta c_{t\max}} \tag{3.28}$$

This factor is required to determine the "in-line" grit spacing, λ. In other words, k_{af} is the required number of *UPV*s existing between the two nearest grits which occupy the same lateral and vertical positions (i.e., "in-line" grits) but different transverse positions. Thus, the "in-line" spacing is defined as

$$\lambda = k_{af} L_{UPV} \tag{3.29}$$

and so,

$$\lambda = \frac{UPV}{\Delta c_t \Delta c_w} = \frac{1}{\gamma_p \Delta c_w \Delta c_{t\max}} = \frac{(1+\beta_s)\pi\rho d_g^3}{6\alpha_c C^* \Delta c_w \Delta c_{t\max}} \tag{3.30}$$

The correct value of λ depends strongly upon $\Delta c_{t\max}$ and Δc_w, and it must be remembered that Δc_w is a function of Δc_t, as given in Eq. (3.19). Thus, accurate values of both of these parameters are essential. An estimate for $\Delta c_{t\max}$ has also been made using several of the known variables, such as grit diameter, amount of grit retention, and amount of grit diameter contact, as shown in Eqs. (3.15) through (3.17). Thus, knowledge of Δr_{Pmin} is very important. So, in the next section, a the numerical computation scheme is developed

to compute Δr_{Pmin} for many cases, and an average value has been taken of the distribution of Δr_{Pmin}.

3.5 Numerical Model

3.5.1 Summary of Approach

The numerical approach also consists of relating grit spacing, λ, to all of the controllable parameters used by tool makers, such as grit concentration and grit size. This approach was implemented using a FORTRAN program named the *DIGS* (DIamond Grit Spacing) Numerical Computation Program. In this approach, a random distribution of grits is numerically generated within a given domain. The segment surface is considered to be the boundary of the domain. A random "slice" (or cross-section) of the segment is then taken. This "slice" is considered to be a random cutting surface which would appear during the sawing operation. With this "slice" the number of grits exposed to the cutting surface can be easily computed. Using a referenced datum line (60% grit retention), such quantities as the number of grits exposed to the surface, as well as the number of "pull-out" grits, may be computed. This is performed by simply examining locations on the surface where the minimum allowable retention percentage has not been exceeded. Also, from the number of grits exposed and the grit height, the number of grits currently active (i.e., "working" grits) or inactive in the cutting process can be determined. The number of grits currently active or inactive in cutting can also be determined using the analytically computed maximum and minimum protrusion height (Δr_{Pmax} and Δr_{Pmin}) information as the differentiating rule. On the average, both methods should yield the same results. Therefore, the analytical basis of Δr_{Pmax} and Δr_{Pmin} will then be used to determine the number of working grits. Thus, with this information the average grit spacing, λ, can be

numerically computed. Also, the *UPV* arrangement factor can be correlated to the findings of the numerical algorithm.

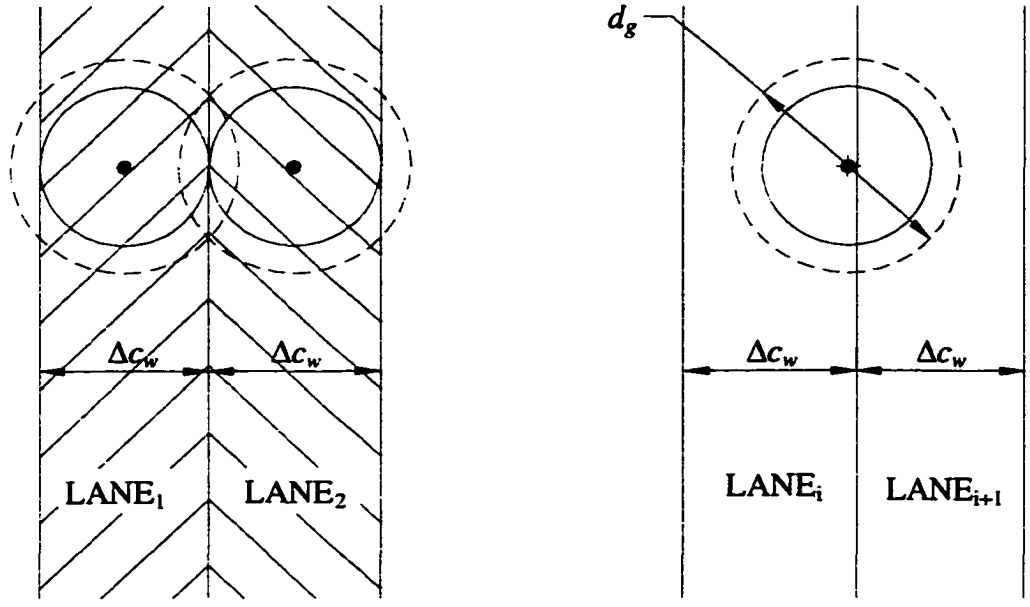

(a) (b)

Figure 3.12 Imaginary "Lanes" of "In-Line" Paths

3.5.2 "In-Line" Path (or Lane) Implementation

In many cases it has been found that the surface data from more than one segment is necessary to compute several values of λ. This is due to the sparcity of exposed grits on one segment which (1) are at the working height, and (2) lie along the same "in-line" path as a neighboring grit. To circumvent this problem, a number of *imaginary "lanes"* are used to represent the different in-line paths (see Figure 3.12). To ensure complete cutting coverage on the segment surface, the average width of cut, Δc_w, is used as the lane width. For the many cases in which a grit overlaps two adjacent lanes, the grit center and the lane boundaries are used to determine the proper lane placement of the grit. Once

proper lane assignments have been made in the algorithm, the FORTRAN code simply computes a local λ value for all adjacent grits lying in the same lane. After all of the λ_{local} values are computed for each lane, the average λ of these values is computed. It is this value which can be compared to the analytically computed value for λ by Eq. (3.30). The flow chart of the *DIGS* algorithm can be found in Appendix C. The information contained in it simply reinforces or restates the discussion given above.

3.6 Results and Discussion of Analyses

Figures 13.13, 13.14, and 13.15 show a plot of the grit spacing parameter λ as a function of concentration C^*. These plots illustrate the usefulness of the analytical and numerical methods developed when specific input parameters are given. Typical sets of input parameters are used and given on the graphs. As expected, the value of λ generally decreases as C^* increases (i.e., is inversely proportional) for both graphs. This simply means that as the number of grits in a segment increases, the spacing between two successive "in-line" grits decreases. Qualitatively, this is no new fact, but the power comes in the ability to predict quantitatively the magnitude of the decrease. The curve becomes increasingly linear near the upper end of the C^* range. However, as the size of the grit d_g increases (i.e., US Mesh Size decreases), the spacing λ tends to increase if the other parameters are held constant. A table of typical concentration values is also presented along with the grit size in micrometers (μm) in Table 3.1.

The analytical model represents "perfect" or ideal cutting. This means all of the cutting portion a grit is used before the next grit (which is vertically lower than the dynamic grit Δc_{max}) begins to make contact (i.e., cut) the workpiece (or ideal utilization of

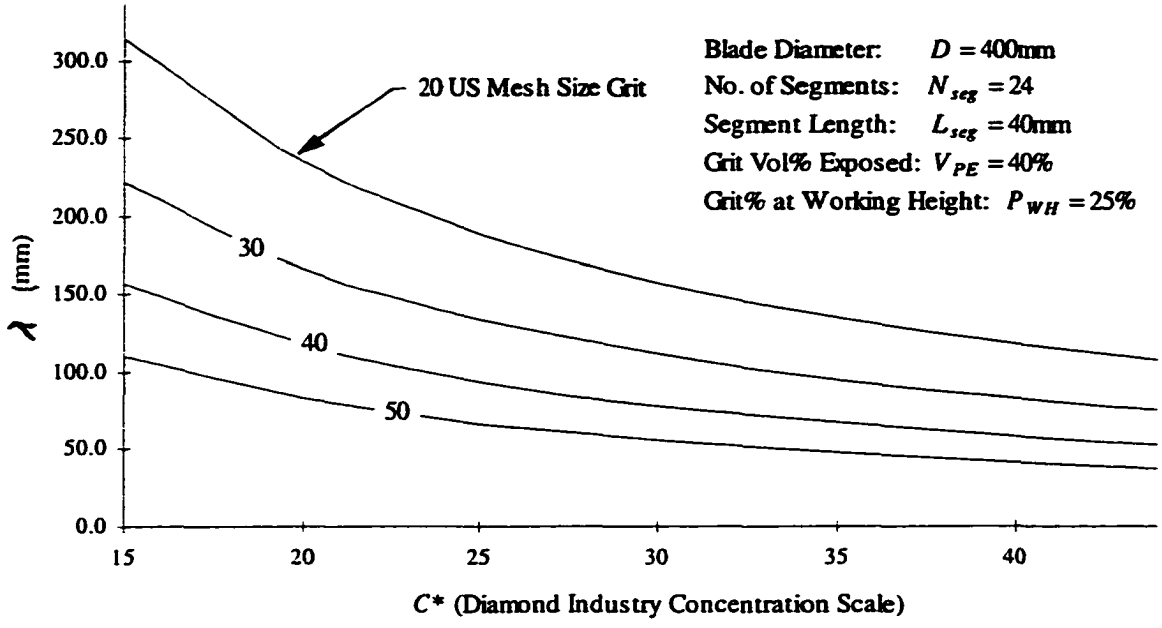

Figure 3.13. Grit Spacing vs. Concentration (Analytical Model)

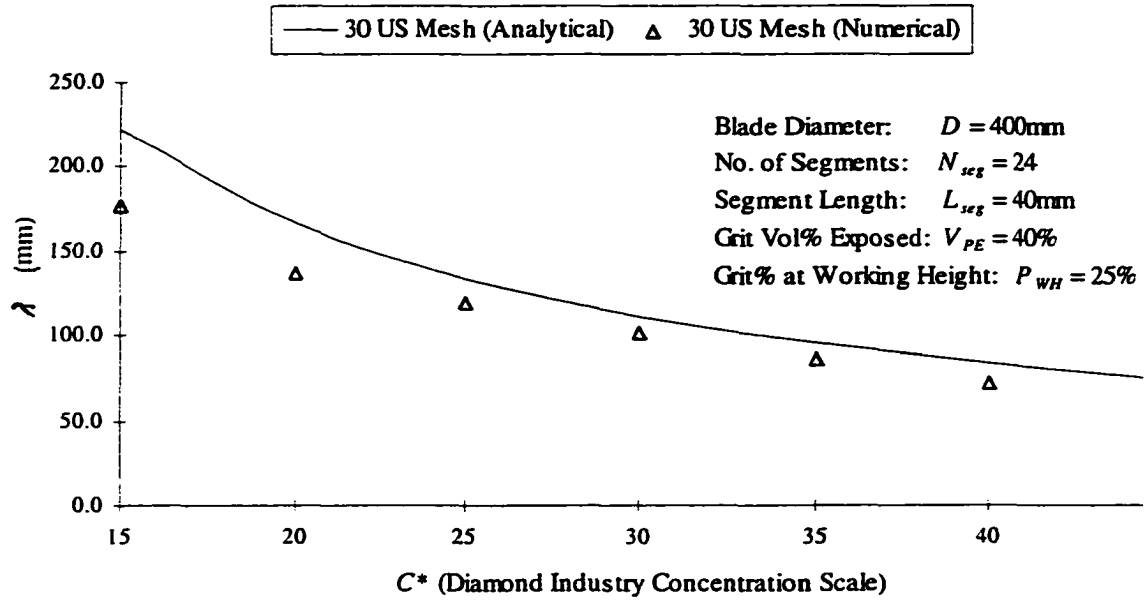

Figure 3.14. Grit Spacing Model Comparison (30 US Mesh)

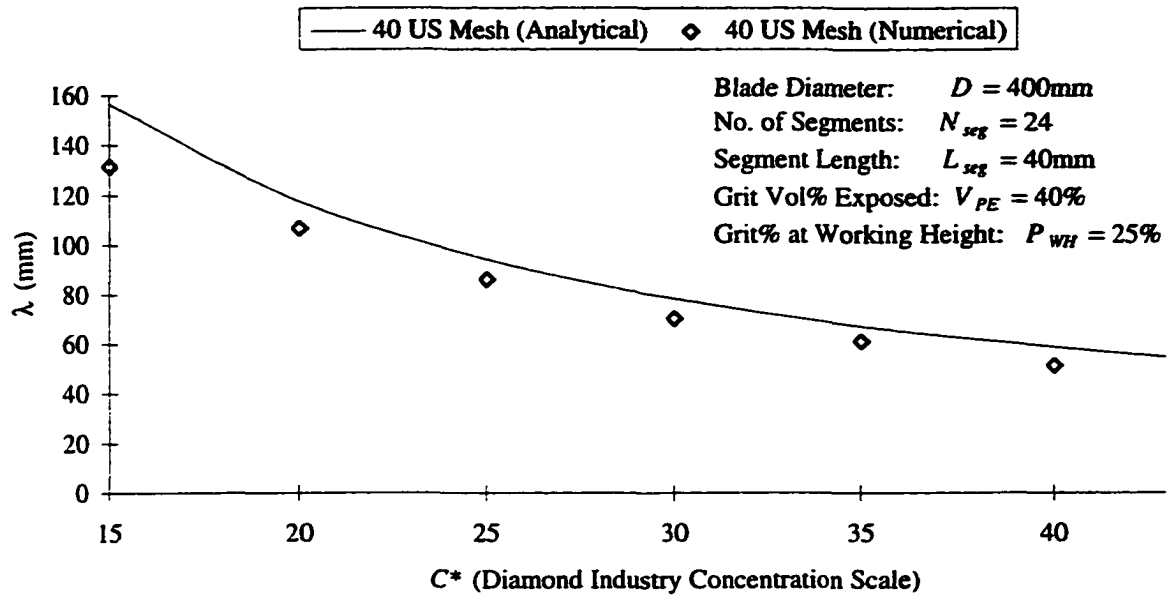

Figure 3.15 Grit Spacing Model Comparison (40 US Mesh)

grits). This assumes that wear for one grit can be defined as the removal by abrasive rubbing or impact of the region of the grit which is located above the Δr_{min} mark of the grit. This "perfect" cutting scenario is not quite true for the actual case, since the grits hold random positions and heights. Thus, ideal grit utilization is not expected, nor is it achieved by the numerical scheme. The graphical results shown in Figures 3.14 and 3.15 indicate that generally the numerical solution is 85 to 95% of the ideal analytical *UPV* model. The margin of difference between the results is fairly uniform, but tends to slightly decrease as the concentration increases. For the 40 US Mesh results at 45 concentration, the difference between numerical and analytical λ values is only 9.2%. On the other end of the C^* range (15 concentration), the maximum difference between the numerical and analytical results occurs (9.7%). So for the conditions considered, there is not a large deviation in percentage difference over the range of C^*. It is believed that this deviation occurs because there are a lower number of grits present in the matrix and on the

segment periphery at lower C^* values. Typically, if more grits are present on the periphery, a better approximation of λ should be made due to the statistics. The data points plotted represent the average of five (5) runs with the computer. So, statistically speaking, this gives a good approximation of a realistic value for λ. Also, since the numerical model more closely represents the actual case, it is recommended that its λ value be used in real life conditions and computations.

Table 3.1

(b)
Typical Concentration Values

Concentration	
C^* Scale or Units	Equivalent mass per unit volume (gm/cm^3)
15	0.132
20	0.176
25	0.220
30	0.264
35	0.308
40	0.352
45	0.396

(a)
Typical Grit Sizes

US Mesh	Average Grit Diameter (μm)
20	841.0
25	707.0
30	595.0
35	500.0
40	420.0
45	354.0
50	297.0

3.7 Comparison with Experimental Data

Unfortunately, experimental measurement of grit spacing can only practically be measured via the surface density parameter C. But as discussed earlier, C generally doesn't take into consideration whether or not the grits are working or non-working (non-cutting). So computation of λ by use of Eq. (2.32) gives an inaccurate value of λ, as will be shown shortly. To show the direct relationship between the number of cutting

points per unit area C and grit spacing λ of the developed analytical model, Eq. (3.30), is algebraic manipulated via Eq. (3.10) to become

$$\lambda = \left(\frac{1}{C}\right)\frac{(1+\beta_s)d_g}{\Delta c_t \Delta c_w} \tag{3.31}$$

Also, the grit spacing equation, that is, Eq. (2.32) cited by many researchers (Malkin, 1989; Li and Liao, 1996) is given again

$$\lambda = \frac{1}{Cr(t_{max}/2)} = \frac{1}{Cw_c} \tag{3.32}$$

where w_c is the chip width at the mean chip thickness ($w_c \cong \Delta c_w$).

Experimental data for C was obtained to compare and verify the results of the presented models (Hayden, 1998). This data was obtained from General Electric Superabrasives, a company that has been performing grit count analysis for many years. The raw data is taken by physically counting the number of diamond grits on the surface of the diamond segment. The counting did not take into consideration the protrusion height of the visible grits. The data is essentially collected for varying concentration and mesh size. Because of the duration of the data collection, many hundreds of segments (if not thousands) have been added to the sample set. The typical segment size for a 400 mm diameter test blade is 4 mm by 25 mm. In the test procedure, several segments are counted and the grit count per unit area is computed. The sample size varies due the diamond distribution variation, but enough grits were counted to obtain a reasonable confidence band (95%). The grit count is performed using an optical microscope at varying magnifications which depend on grit size. For example, a 40/50 US Mesh would typically require a 20X magnification. A finer grit, such as a 70/80 US

Mesh, requires the higher resolution of 50X magnification. The amount of wear which was allowed before the observation also varied, but segments are allowed to wear at least 1 mm before surface analysis is performed. Computer models which compute grit surface count or density have also been developed (Hayden, 1998; Koshy, 1993). Their models also assume the grits to be spheres having an average diameter. At least one model has also been refined to account for the diamond morphologies and the range of diameters in a given size range. The fit of the models with the experimental data for C is not exact, but it is essentially the same.

To compare the developed models and the experimental data, the surface density is plotted against concentration, as shown in Figure 3.16 for two different mesh sizes. Both experimental data and developed model (that is, the model used to derive Eq. 3.10), shows the linear relationship between concentration and grit count density. The graph indicates a nearly perfect agreement for the 30 US Mesh across the entire concentration range. The greatest deviations seem to occur at the higher mesh size (i.e., smaller grits). Nevertheless, the maximum deviation is only 17%. In Figure 3.17, the grit spacing parameter from the different models and experimental data is displayed for a constant mesh size (30 US Mesh). The results indicate excellent agreement between the experimental values of the λ as well as the numerical and analytical models. The graph also displays λ computed by Eq. (3.32). It shows that this equation severely underestimates λ when a non-adjusted C value is used. For that equation, the C quantities must be greatly adjusted (i.e., decreased to 12 to 20% of its value) to correspond to the other curves. It must also be stated that the presented λ graphs are strongly a function of the percentage of grits at the working height P_{WH}. Future studies

should seek to examine this parameter more closely. But in summary, the developed models presented indicate that they can accurately predict the grit spacing value of working grits. Thus, the number of actively working (or cutting) grits can be predicted, and the average grit load can be computed if the resultant load is known from experiments.

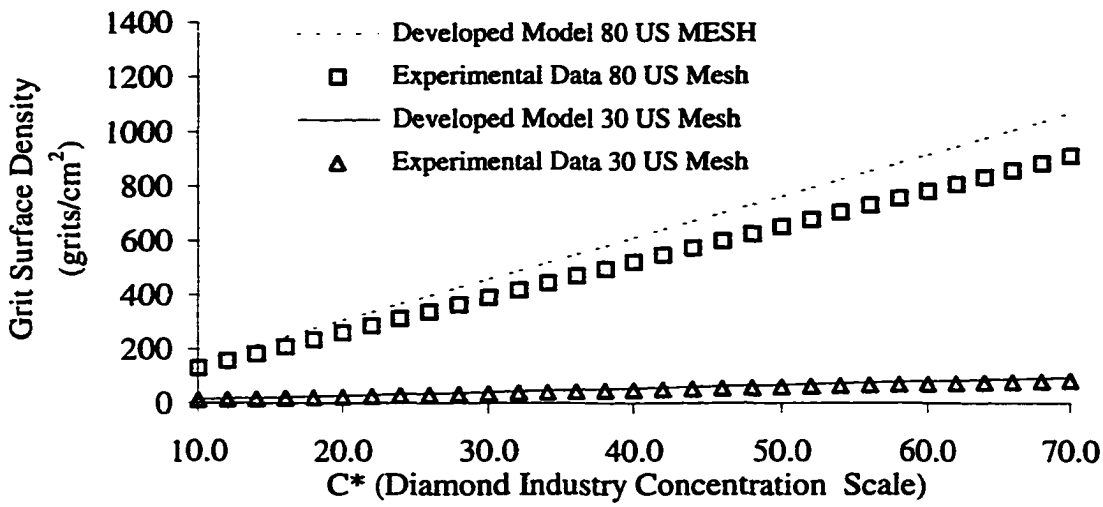

Figure 3.16 Grit Surface Density - Experimental Data and Developed Model (Eq. 3.10) Comparison.

3.8 Summary

What does all of this information mean to diamond tool makers? It means that they can determine exactly the average spacing λ of the grits making contact with the workpiece based solely on controllable tooling parameters, such as grit size and concentration. This ability to slightly modify λ will in turn mean the modification of the cutting forces developed. Much of the common information has been known in the past in general (or arbitrary) terms, but now a model has been developed which quantifies and

unifies many different aspects of the sawing process. And as noted earlier, the computation of λ will also allow the explicit computation of t_c, the mean chip thickness.

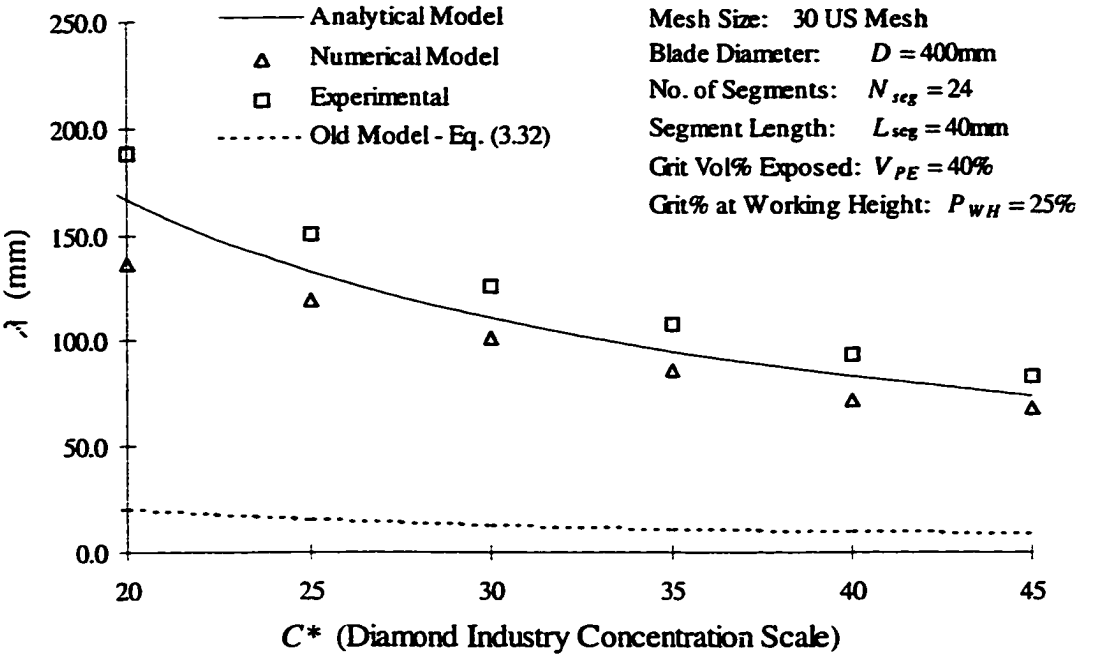

Figure 3.17 Grit Spacing Models and Experimental Data Comparison for a 30 US Mesh Size.

CHAPTER 4

SAW BLADE FINITE ELEMENT ANALYSIS

4.1 Introduction

As mentioned in Chapter 1, the circular diamond saw blade consists of the diamond segment and the blade core (or hub) as its two major components. This segment is usually mounted to the periphery of the blade core by brazing. The blade core is fabricated from sheet steels having a thickness ranging from approximately 1 to about 10 mm. This range will vary for different manufacturers. The core is mounted and clamped to the cutting machine's spindle with a flange(s). These cores are work hardened by pre-stressing methods to offset stresses produced by centrifugal, heat, and cutting forces. Hence, reducing any of these forces means the blade's stability is improved, vibration is reduced, and more efficient cutting can be achieved (Büttner and Mummenhoff, 1973).

Normal circular saws possess cutting edges (teeth) along a continuous periphery. However, the diamond circular saw consists of a number of small slotted sections equally spaced around the periphery of the blade, as shown in Figure 2.1. These slots aid in the removal of debris during the cutting operation, and they enable an adequate flow of coolant to reach the cutting zone. This means a larger cooling area will exist, and a temperature increase will be deterred. They also prevent distortion of the blade core during the brazing of the diamond segment to the surface. The quality of the cut is also affected by these slots. Smaller slot widths promote cleaner and more precise cuts than

wider slots, while as would be expected, having wider slots produces better debris removal (Wilks, and Wilks, 1991; Mahomed et al., 1972).

However, one drawback of slots is the introduction of geometrical discontinuities along the blade periphery. Thus, when peripheral loadings (i.e., cutting forces) are applied, these discontinuities become areas of stress concentration, which have an adverse effect on the life and performance of the blade. In the work performed by Mahomed et al. (1972) the problem of fatigue cracking in the slot area of the blade core was examined. The goal of their study was to increase the core's fatigue life through varying the slot shape. The effect of slot shape variation was studied using the finite element method. They determined that this variation does in fact affect the fatigue stress of the blade. The following sections of this chapter discuss the stress concentrations which are developed when several slot parameters, which are to be defined later, are varied. The goal of this analysis is to locate the area of highest stress and to find the parameter values which minimize this stress. The finite element method will be the tool used to model the induced blade forces and compute the stresses.

4.2 Finite Element Analysis

The cutting process occurring during sawing has been discussed in Section 2.2 of Chapter 2. It was noted that the segment surface grits remove material through scratching and cracking the workpiece surface, thus producing chips and deformation. Forces and very complex compressive and shear stresses are developed along the diamond segment/workpiece surfaces. Furthermore, these contact forces and stresses are transferred through the segment to the blade core. It is these forces which will be used to perform the stress analysis of the blade.

Finite element software COSMOS/M was utilized to perform the finite element analysis (Structural Research and Analysis Corp., 1993). A four-node, 2-D plane stress element was used. The mesh was refined around the slot holes where the stress concentration is expected. As shown in Figure 4.1, the element size along the periphery of the blade becomes smaller toward the slot sides. The spacing ratio of the mesh design is 0.2 on the side of the periphery. In order to compare the performance of the saw blade, constant cutting forces, 600 N in the radial direction and 100 N in the tangential direction, are assumed (Liao and Luo, 1992). The work by Brach et al. (1988) shows that the cutting forces generated during sawing do reach a steady-state value after initial segment "wearing in" occurs. The results of Ertingshausen (1985) also show that this is factual. He also found that the cutting forces stabilize after an initial transient force period. These are the justifications used to establish the usage of a constant loading force. The cutting forces are also assumed to be uniformly distributed on the surface of contact.

Knowing that the cutting process is a continuous motion of the saw blade, the loading condition is a function of time. Ideally, all possible loading conditions, due to different positions of the blade, need to be investigated in order to determine the maximum stress. However, when the contact region contains the entire slot, the contact area becomes the minimum such that the maximum cutting stresses are reached. As shown in Figures 4.2 through 4.4, three load cases are considered as critical loading conditions for the comparison of the maximum stress within the saw blade. Hence, critical stress concentration conditions can be found from either of these three loading conditions.

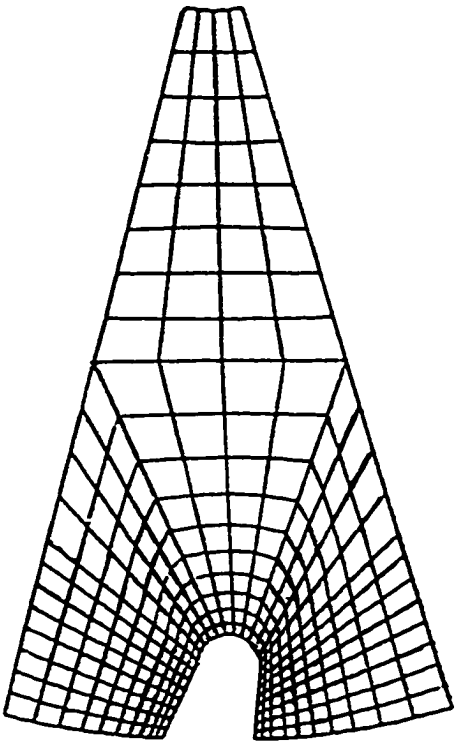

Figure 4.1 Example of a Typical Finite Element Mesh Used in Stress Analysis

1. Load Case No. 1: Under this loading situation, as shown in Figure 4.2, the slot is at the left end of the contact region. This causes the cutting stresses to be concentrated on the segment of the saw blade to the right of the slot. The maximum stress is expected to lie along the right perimeter of the slot hole.

2. Load Case No. 2: Under this loading situation, the slot is at the right end of the contact region, as shown in Figures 4.3. This causes the cutting stresses to be concentrated on the segment of the saw blade to the left of the slot. The maximum stress is expected to be located along the left perimeter of the slot hole.

3. Load Case No. 3: As shown in Figure 4.4, under this loading situation, the slot

is located at the center of the contact region. This causes the cutting stresses to be concentrated at the openings of the slot.

Area of contact is determined from the depth of cut and the blade diameter. The nodal forces are calculated based on the uniformly distributed cutting stress over the area of contact and the element sizes. All the above load cases include the centrifugal force which is due to the rotation and the density of the blade. A constant angular velocity, ω, 104.7 rad/s (1000 rpm), is applied for all the load cases. Since the core materials used for the blade are usually ductile metal materials, von Mises stress Y is used as the objective function and is to be minimized. Where

$$(\sigma_1-\sigma_2)^2+(\sigma_2-\sigma_3)^2+(\sigma_3-\sigma_1)^2 = 2Y^2 \tag{4.1}$$

and σ_1, σ_2 and σ_3 are the three principal stresses.

4.3 Optimization Approach

As shown in Figure 4.5, the shape of the blade and the slot can be described by the following parameters:

D: blade diameter

r: radius of slot base circle

γ: slope of slot

ϕ: angle between the left slot side and the direction of the slot

ψ: angle between the right slot side and the direction of the slot

Listed below are some of the sawing parameters that are kept constant during the optimization approach (IMEX International, 1993):

D: blade diameter (200 mm)

h: depth of cut (2 mm)

t: blade thickness (1.8 mm)

s: distance between the center of the slot base circle to the periphery of the blade (8.5 mm)

w: slot width (7.0 mm).

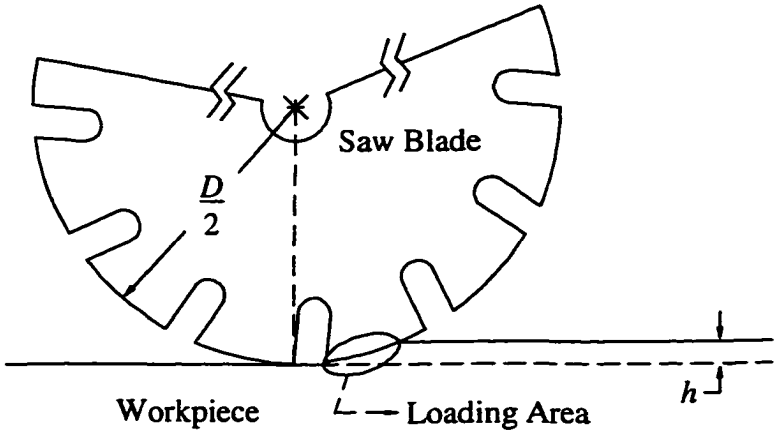

Figure 4.2 Load Case No. 1

During the optimization approach, γ is the first parameter being studied. After the optimal angle for γ has been decided, an attempt to change r will be made. Finally, both ϕ and ψ will be altered to obtain the best stress distribution.

4.4 Results and Discussion

For each blade configuration under each load case, the maximum von Mises stress within the blade is located and its value is obtained. Table 4.1 and Figure 4.6 show how

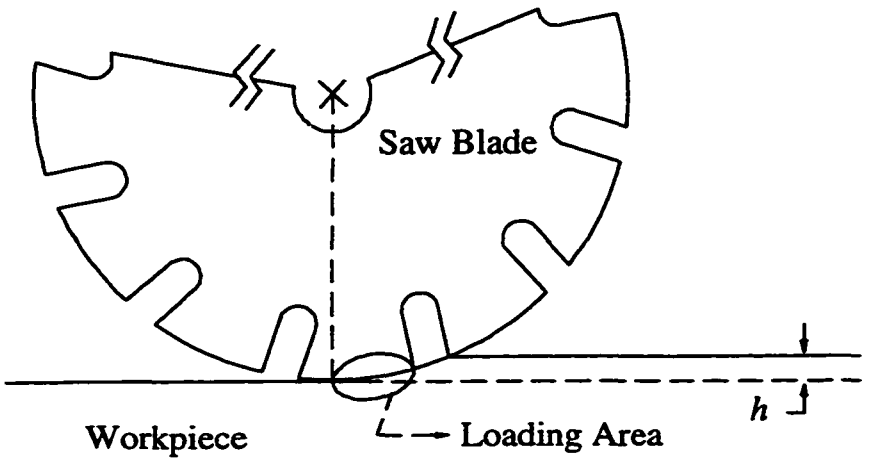

Figure 4.3 Load Case No. 2

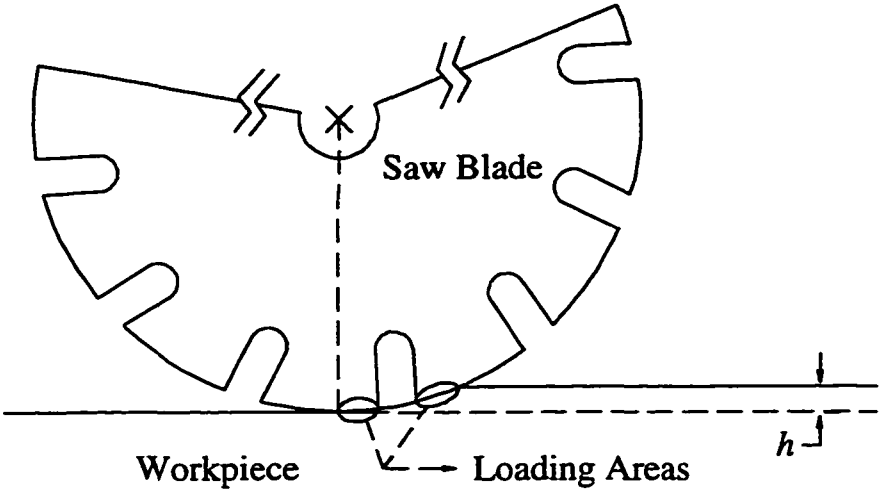

Figure 4.4 Load Case No. 3

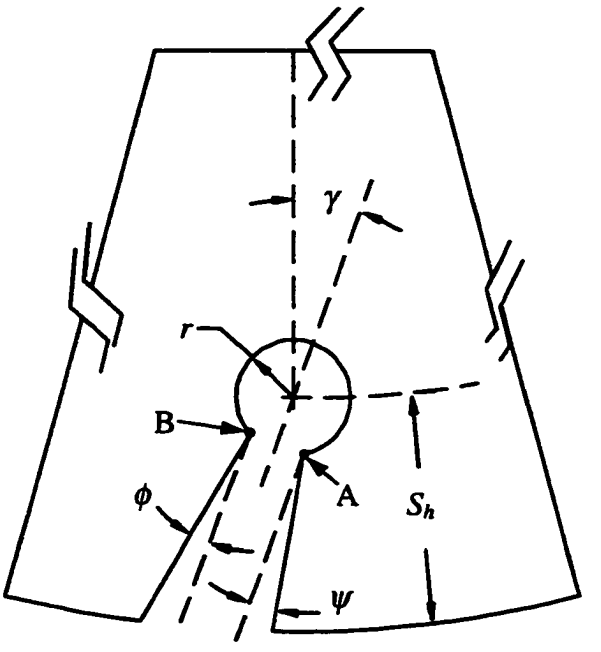

Figure 4.5 Illustration of Slot Parameters

the slot angle γ affects the maximum von Mises stress for each load case. Intuitively, the increase of the slot angle γ increases the "stress absorption area" to left of the slot for load case No. 2 but reduces the "stress absorption area" to the right of the slot for load case No. 1. The "stress absorption area" receives this label because it distributes the stress from the blade periphery to a larger area. Also when load case No. 1 is applied, a larger slot angle will result in a reduced bending rigidity of the protruding triangular portion of the blade; hence the stress becomes larger. This intuition is shown to be correct from Figure 4.6, where the increase of γ increases the maximum von Mises stress for load case No. 1 but decreases the stress for load case No. 2. Load case No. 3 always results in non-crucial maximum von Mises stresses. Hence load case No. 3 is applied to only several blade geometries. The optimal slot angle, γ, which can be seen from Figure 4.6, is 10°. This is the optimal angle because it produces the overall minimum value of the maximum stresses under the three load cases.

Table 4.1 Maximum Von Mises Stress for Varying γ

γ (degrees)	Load Case No. 1 (MPa)	Load Case No. 2 (MPa)	Load Case No. 3 (MPa)
0	52.7	80.1	53.0
5	59.6	73.3	--
10	67.5	67.0	50.1
20	88.2	55.5	68.0
30	120.4	44.8	--

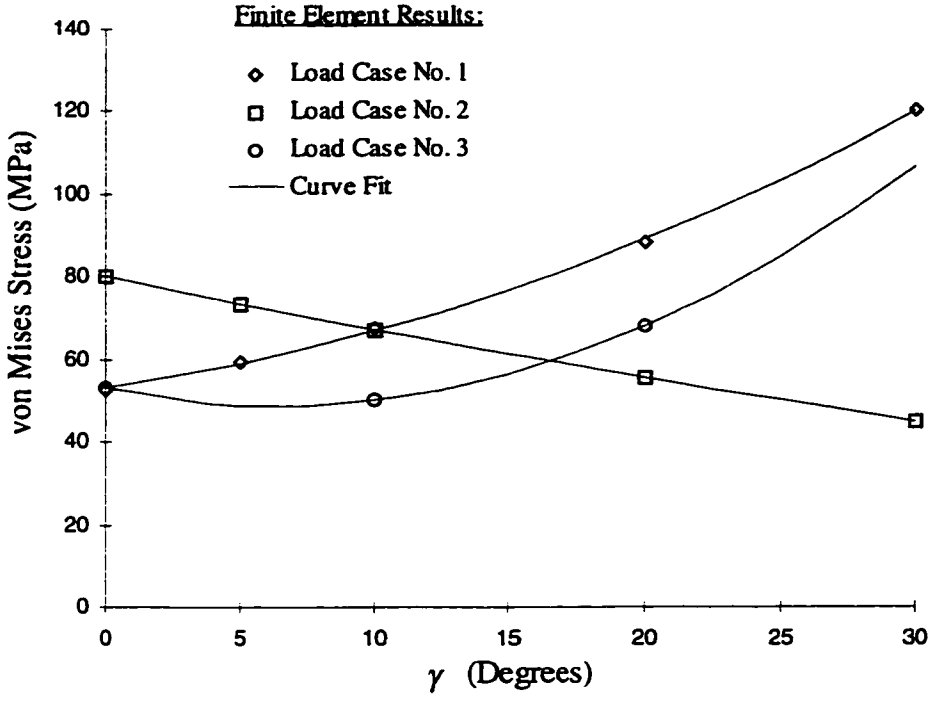

Figure 4.6 Plot of Finite Element Results with the Maximum von Mises Stress vs. Angle γ

Examining the results from different slot angles, the maximum von Mises stresses under either load case No. 1 or No. 2 are all located at the periphery of the slot base circle and are near the slot side and circle intersection. These locations are labeled as points A

and B in Figure 4.5. It was thought that increasing the radius of the slot base circle might better distribute the concentrated stress. However, as shown in Table 4.2, the results indicate that the increase of the radius will increase the stress concentration since the stress absorption area is decreased

Table 4.2 Maximum von Mises Stress for varying r with $\gamma = 10°$

r (mm)	Load Case No. 1 (MPa)	Load Case No. 2 (MPa)
3.5	67.5	67.0
4.0	74.9	72.8
4.5	79.1	75.3

After the slot angle and the radius of the slot base circle have been determined, varying the angle ϕ between the left slot side and the slot direction and the angle ψ between the right slot side and the slot direction is also necessary to further reduce the maximum stress. The results for different combinations of the two angles are shown in Table 4.3. It is found that the best combination of ϕ and ψ is 5° and 5°, which produces the maximum von Mises stresses 61.2 MPa for load case No. 1 and 63.6 MPa for load case No. 2. This non-zero combination of ϕ and ψ further reduces the maximum von Mises stress for load cases No. 1 and No. 2 by 6.3 and 3.4 MPa, respectively.

In summary, it has been shown that with the proper design, the maximum stresses within a blade can be minimized. Furthermore, when the blade receives lower stresses its fatigue life should increase as well as its performance. This will benefit the end users of the blade and will lower their tooling costs.

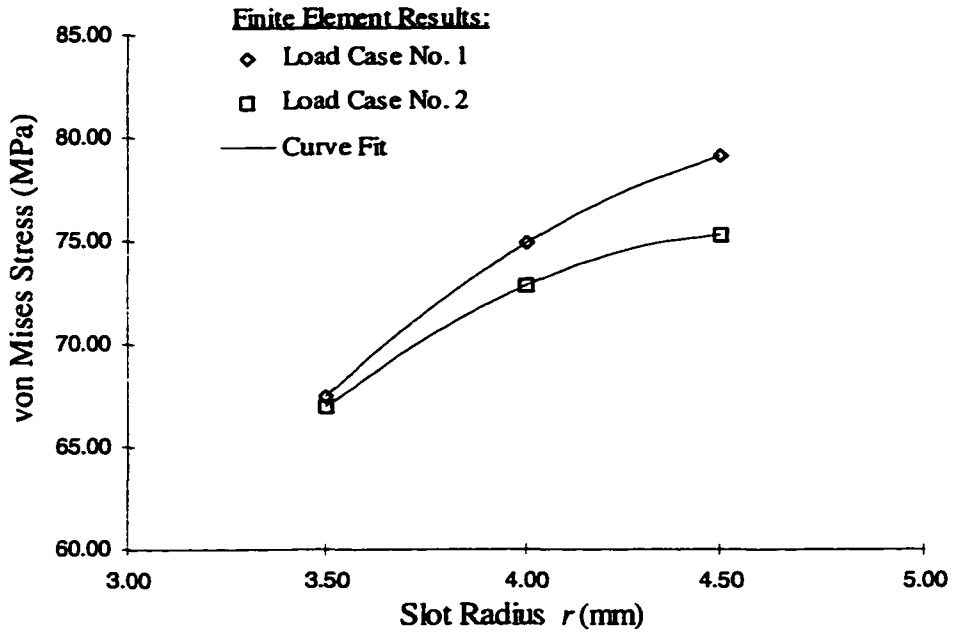

Figure 4.7 Plot of Finite Element Results Showing the Variation of the Maximum von Mises Stress with the Slot Radius r

Table 4.3 Maximum von Mises Stress for varying ϕ and ψ with $\gamma = 10°$ and $r = 3.5$ mm

ψ (degrees)	ϕ (degrees)	Load Case No. 1 (MPa)	Load Case No. 2 (MPa)
0	0	67.5	67.0
5	5	61.2	63.6
10	10	65.7	62.0
5	15	73.6	57.0
3	20	78.1	52.9
10	20	69.2	55.0

CHAPTER 5

CONCLUSIONS AND RECOMMENDATIONS

5.1 Kinematics Analysis

As a result of this work, chipping geometries have been mathematically defined and derived. These geometries are bounded by four curves and are functions of the independent machining parameters h, D, v_T, v_P, and λ. From the knowledge of the chipping geometries, chip area and mean chip thickness relations have been obtained. And an expression for the thickness-spacing ratio t_c/λ was derived as a function of only the depth-diameter K_1 and speed K_2 ratios. Since the relative cutting force, f_r, is proportional to the chip thickness by some power, n, the factors affecting this force can be identified. A graph of the t_c/λ expression was provided to investigate the effects of the machining parameters. It was shown that t_c/λ curves increase as K_1 and K_2 increase. More specifically, it was found that increasing v_P and D reduces the mean chip thickness. Contrarily, increasing v_T, h, and λ increases the magnitude of the mean chip thickness.

Next, the earlier maximum chip thickness, t_{max}, models were reviewed. To compare these models with the proposed model, the t_{max} expressions were converted to equivalent mean chip thickness, t_c, equations. It was also found that all of the different t_{max} expressions simplify to the same t_c equation. The graph generated for the new model and the equivalent t_c/λ value from the earlier models show an excellent agreement for the lower end of the K_1 range, as expected. However, a small discrepancy

manifests and increases as K_I increases. The primary cause of this discrepancy has been attributed to the small angle approximations made in the derivation of the t_{max} in the older models. Thus, it is evident that the new model or the alternative method should produce more accurate t_c values at moderate to large K_I values, which should be expected in the sawing operation. This fact also has a practical significance on the computation of the grit force and grinding ratio, in that more accurate values of these parameters can also be expected.

5.2 Grit Distribution Analysis

An analytical and numerical model has been presented which determines the average grit spacing, λ, for the diamond saw blade cutting operation. This term represents the spacing of successive "in-line" grits located on the segment surface which are actually making contact with the workpiece. Many authors in the past, Opitz et al. (1972), Brecker and Shaw (1974), etc., have referred to this type of spacing as "dynamic." This type of definition is necessary because there are also grits on the segment surface which are exposed to the surface but make no contact with the workpiece. These exposed non-working grits, along with the "dynamic" grits, have been jointly termed as "static."

The analytical method uses the assumption that the diamond segment possesses a uniform (or pseudo-uniform) distribution of particles. To accomplish this task, an abstract entity called a unit particle volume (*UPV*) was introduced, which physically represents the "effective" volume one grit occupies. An appropriate stacking procedure in the lateral and vertical directions for the *UPVs* was then formulated so that complete coverage of the cutting surface would be achieved. The vertical stacking ensures that this complete coverage is maintained for "any" horizontal plane within the segment

which in the future will become the cutting surface. In other words, the *UPV* handles the three-dimensional (or spatial) aspects of the grits in the segment.

However, the numerical method uses a realistic random distribution of particles approach coupled with a "brute-force" method of computing a value for λ. In this approach a random distribution of grits is numerically generated within the segment domain. The program takes a random "slice" of the domain which represents the cutting surface. Using the appropriate parameters (e.g., grit retention percentage, working height percentage, etc.) it determines which surface grits have enough exposure to make contact with the workpiece. These grits contacting or "dynamic" grits are then grouped into lanes so that successive grits can be identified and their local spacing value, λ_{local}, can be computed. The average of these local spacing values is taken for each lane on an individual segment and the total number of segments on one blade. This average represents the λ value reported in the results.

A comparison was also made to verify the results of these methods. As expected, the results indicate that the value of λ is inversely proportional to C^*. Qualitatively, this is no new fact, but the ability to predict quantitatively the magnitude of the change in λ is very beneficial. The graphical results indicate that generally the numerical solution is 85 to 95% of the ideal analytical *UPV* model. This is excellent agreement for the models and underscores the validity of both approaches. Experimental data was also obtained to validate the proposed models. The results show good agreement between the experimental and models' results. Since the numerical model represents the actual cutting surface a more accurately (i.e., random) than the analytical model, it is recommended that its λ value be used in actual computations.

When coupled with the chip thickness-grit spacing ratio equation, an explicit numerical value of chip thickness t_c can be computed. For example, if (1) the force required to produce one chip is known, (2) the number of active cutting grits spanning across the width of the segment is known, and (3) the periodicity of chipping occurrence is known, then all of the grit forces across the surface can be summed to determine a resultant sawing force. The periodicity of chipping is the time in which a chipping process occurs and depends upon the machining parameters, such as, peripheral speed v_P, traverse speed v_T, depth of cut h, and blade diameter D, as well as the segment material property, and grit spacing, λ (a function of concentration, grit size, etc.).

It is also believed that the information provided will enable tool manufacturers to better tailor their diamond segment products to meet customer needs. This can be accomplished by determining the optimal grit spacing which provides maximum usage of the diamond grit during sawing. Incorrect spacing (or grit surface distribution) can lead to either not enough working grits resulting in excessive matrix wear and dull cutting. Incorrect spacing can also produce to too many surface grits which leads to high diamond consumption and non-optimal grit usage. Thus, the developed λ models, analytical and numerical, can search for this optimal spacing as a function of concentration and grit size.

5.3 Saw Blade Finite Element Analysis

Lastly, a finite element analysis of the saw blade was performed in search of an optimal design. The results are based on the assumed cutting force and an assumed uniform cutting stress distribution. The optimal slot angle as well as the offset angles of the slot sides were obtained through this study. Knowing that the cutting force would be

different for any change of the cutting parameters, the results of the present paper can be utilized only when the cutting stresses are uniformly distributed along the blade periphery and the total cutting forces are 600 N and 100 N in the radial and tangential direction, respectively. The angular velocity of the blade used for this study is restricted to 1000 rpm. However, this study shows the existence of the optimal design of the blade geometry. It also shows that the finite element analysis can determine the design parameters which produce a minimum stress concentration. In turn, this optimal design will lead to an increased saw blade fatigue life. This study was focused on the optimization of the blade design from the mechanical loadings only. Other design criteria, such as thermal stress, heat dissipation, etc., would be necessary if these factors are considered. It is recommended that an experimental case studies be performed to further validate these findings in the future.

To further utilize the concept of the optimal design, the cutting force needs to be well formulated as well as the cutting stress distribution. Past studies have been underway to relate and verify the previously mentioned cutting parameters to the cutting force via the chip thickness (Tönshoff and Warnecke, 1982; Jerro, 1995). Hopefully, future studies will quantitatively determine the coupling relationships between the cutting force and blade geometry using the finite element approach. Different types of cutting force, such as those which produce uniform and non-uniform stress distributions, could then be used for analyzing the optimal blade design.

5.4 Final Words and Recommendations

The diamond blade sawing is a incredibly complex process. There are tens of parameters, if not more, involved and micro- and macroscopic phenomena which occur

during sawing which specifically span the entire mechanical, thermal, and chemical fields. It has been endeavored to address only a couple of the key issues which pertain to the process. It has been long believed that no one model can fully address all of the intricacies and physical phenomena involved in such a process. And to further complicate these issues, most of the quantities discussed are extremely difficult to experimentally verify. Hence, as seen with this study, relationships and quantities have to be acquired through other measurable parameters. To shed a little light on this bleak picture that has been painted, it is the author's opinion that with the rise of powerful of modern computers and computational mechanics, a good "all encompassing" model will be developed which will do what at one time was thought "impossible." It is hoped that this work provides a basis for future studies in this fascinating area and will contribute to the goal of creating a non-empirical "all encompassing" model of diamond blade sawing.

REFERENCES

Backer, W. R., E. R. Marshall, and M. C. Shaw, "The Size Effect in Metal Cutting," *Transactions of the ASME*, Vol. 74, Jan. 1952, pp. 61-72.

Bailey, M. W., and G. J. Bullen, "Sawing in the Stone and Civil Engineering Industries," *Industrial Diamond Review*, Feb. 1979, pp. 56-60.

Bailey, M. W., and N. D. Collins, "Investigations Into Diamond Sawing Using Titanized Grits," *Stone Industries*, Stone Industrial Publications Ltd., London, Nov./Dec. 1977, pp. 18-21.

Beitz, W., and K.-H. Küttner, *Dubbel: Handbook of Mechanical Engineering*, Springer-Verlag Ltd., London, 1994, pp. K50-54.

Beyer, W. H., ed., *CRC Standard Mathematical Tables*, 26th ed., CRC Press, Inc., Boca Raton, FL, 1981, pp. 414-417.

Beyer, W. H., ed., *CRC Standard Mathematical Tables*, 29th ed., CRC Press, Inc. Boca Raton, Florida, 1991, pp. 111.

Boothroyd, G., and W. A. Knight, "Grinding", in *Fundamentals of Machining and Machine Tools*, 2nd ed., McGraw-Hill, New York, 1989, pp. 281-291.

Brach, K., D. M. Pai, E. Ratterman, and M. C. Shaw, "Grinding Forces and Energy," *Journal of Engineering for Industry* Vol. 110, Feb. 1988, pp. 25-31.

Brecker, J. N., and M. C. Shaw, "Measurement of the Effective Number of Cutting Points in the Surface of a Grinding Wheel," *Proceedings of the International Conference on Production Engineering*, Tokyo, Japan, 1974, pp. 740-745.

Burgess, R. R., and J. D. Birle, "Circular Sawing Granite with Diamond Saw Blades," *30th Ann. Meeting and Seminar of the Industrial Diamond Association (IDA) of Japan*, Tokyo, May 1978, GE Catalog No. SMD83-517.

Büttner, A., and H. Mummenhoff, "Testing the Stress in Diamond Circular Saw Blades for Sawing Natural Stones and Concrete," *Industrial Diamond Review*, Vol. 33, 1973, pp. 376-379.

Büttner, A., "Diamond Tools and Stone," *Industrial Diamond Review*, Vol. 34, March 1974, pp. 89-93.

Ertingshausen, W., "Wear Processes in Sawing Hard Stone," *Industrial Diamond Review*, Vol. 45, No. 5, 1985, pp. 254-258.

Grisbrook, H., "Cutting Points on the Surface of a Grinding Wheel and Chips Produced," *Advanced. Machine Tool Design Research* , 1962, p. 155.

Hayden, S., Personal communication with Dr. Steve Hayden, MBS Product Technical Manager, General Electric Superabrasives, 1998.

Jennings, M., and D. N. Wright, "Guidelines for Sawing Stone," *Industrial Diamond Review*, Vol. 49, No. 2, 1989, pp. 25-30.

Jerro, H. D., C. Yang, S. S. Pang, and R. A. Mirshams, "Kinematic Analysis of Chipping Materials Using Superabrasive Diamond Tools," *Proceedings of the ASME/ETCE 1995 Energy-Sources Technology Conference & Exhibition*, Houston, Texas, Jan. 29, 1995.

Jerro, H. D., C. Yang, S. S. Pang, and R. A. Mirshams, "Stress Analysis of the Chipping Process of Superabrasive Diamond Blades," *Society of Engineering Science 32nd Annual Technical Meeting*, New Orleans, Louisiana, October 1995.

Jerro, H. D., C. Yang, S. S. Pang, and R. A. Mirshams, "Grit Distribution in Superabrasive Diamond Sawing," *International Journal of Advanced Manufacturing Systems*, Vol. 1, Issue 1, pp. 25-38, 1998 (also published in the *Symposium on Composite Materials, Design and Analysis: Energy Week Conference & Exhibition*, Houston, Texas, Jan. 27-31, 1997).

Jerro, H. D., C. Yang, S. S. Pang, and R. A. Mirshams, "Kinematics of the Chipping Process Using Circular Diamond Saw Blades," in Press, *ASME Trans. Journal of Manufacturing Science and Engineering*, 1999.

Kalpakjian, S., *Manufacturing Processes for Engineering Materials*, Addison-Wesley Publishing Company, Reading, Massachusetts, 1984, pp. 562-567.

Koshy, P., V. K. Jain, and G. K. Lal, "A Model for the Topography of Diamond Grinding Wheels," *Wear*, Vol. 169, No. 2, 1993, pp. 237-242.

Konstanty, J., "The Materials Science of Stone Sawing," *Industrial Diamond Review*, Vol. 51, No. 1, 1991, pp. 27-31.

Li, K., and T. W. Liao, "Modelling of Ceramic Grinding Processes: Part I. Number of Cutting Points and Grinding Forces Per Grit," Wear, Vol. *Journal of Materials Processing Technology*, 1996, pp. 1-10.

Liao, Y. S., and S. Y. Luo, "Wear Characteristics of Sintered Diamond Composite During Circular Sawing," *Wear*, Vol. 157, 1992, pp. 325-337.

Liao, T. W., K. Li, S. B. McSpadden, Jr., L. J. O'Rourke, Wear of Diamond Wheels in Creep-Feed Grinding of Ceramic Materials I. Mechanisms, *Wear*, Vol. 211, 1997, pp. 94-103.

Malkin, S., *Grinding Technology: Theory and Applications of Machining with Abrasives*, Ellis Horwood, Chichester, UK, 1989.

Löns, H. H., "Basic Research on Frame Sawing with Diamond Blades," Dissertation T. U. Hanover, 1970.

Marshall, E. R., and M. C. Shaw, "Forces in Dry Surface Grinding," *Transactions of the ASME*, Vol. 74, Jan. 1952, pp. 51-59.

McGowan, J., and G. Brauninger, "The Application of Superabrasives in Granite Slabbing," *Superabrasives Conference*, Technical Paper MR91-167, Society of Manufacturing Engineers, Chicago, Illinois, 1991.

Mirshams, R. A., K. Crosby, and M. Thomas, "Study of the Co-WC/Diamond Interface and Wear Characteristics in Hot-pressed Composite Tools," Report to the Louisiana Board of Regents and SEA Diamond Tools USA, Inc., Sept. 1994.

Mahomed, M., M. C. deMalherbe, M. A. Dokainish, and R. B. Young, "Stress Analysis of Segmented Circular Sawblades, *Proc. 13th Intl. Machine Tool Design and Research Conf.*, Birmingham, U.K., Sept. 1972, pp. 247-252.

Oliveira, J. F. G., E. C. Bianchi, and G. F. Souza, "G Ratio Optimisation of ABN360 Resin-Bond Wheels," *Industrial Diamond Review*, Vol. 54, No. 561, 1994, pp. 84-87.

Opitz, H., W. Konig, and G. Werner, "Kinematics and Mechanics in Grinding with Regard to the Machining Process," in *New Developments in Grinding*, ed. M. C. Shaw, Carnegie Press, Pittsburgh, Pennslyvania, 1972, pp. 259-282.

Pai, D. M., "A Fundamental Study of the Diamond Sawing of Rock," Ph.D. Dissertation, Arizona State University, May 1987.

Pai, D. M., E. Ratterman, and M. C. Shaw, "Grinding Forces and Energy for Brittle Materials," *Proc. Intersoc. Sym. on Machining Advanced Ceramic Materials ASME*, 1988, pp. 99-111.

Peklenik, J., "Ermittlung von geometrischen und physikalischen Kenngrössen für die Grundlagenforschung des Schleifens," Dissertation TH Aachen, 1957.

Reichenbach, G. S., J. E. Mayer, S. Kalpakcioglu, and M. C. Shaw, "The Role of Chip Thickness in Grinding," *Transactions of the ASME*, Vol. 78, May 1956, pp. 847-859.

IMEX International, Inc. (Formerly: Sea Diamond Tools USA, Inc.), *Technical Product Guide*, Elberton, Georgia, 1993.

Shaw, M. C., "Fundamentals of Grinding," in *New Developments in Grinding*, ed. M. C. Shaw, Carnegie Press, Pittsburgh, Pennsylvania, 1972, pp. 220-258.

Shaw, M. C., "Principles of Material Removal," Vol. 1, ICM 3, Cambridge, England, Aug. 1979, pp. 227-253.

Snoeys, R., J. Peters, and A. Decneut, "The Significance of Chip Thickness in Grinding," *Annals of the CIRP*, Vol. 23, No. 2, 1974, pp. 227-237.

COSMOS/M Finite Element Analysis System, Version 1.65, Structural Research and Analysis Corporation, 1993.

Tönshoff, H. K., and G. Warnecke, "Research on Stone Sawing," in *Advances in Ultrahard Materials Applications Technology*, Vol. 1, ed. P. Daniel, Hornbeam, England, 1982, pp. 36-49.

Tönshoff, H. K., and R. Schulze, "The Effect of the Coolant in Sawing Hard Stone," in *Advances in Ultrahard Materials Application Technology*, Vol. 1, ed. P. Daniel, Hornbeam, England, 1982, pp. 50-62.

Wilks, J. and E. Wilks, *Properties and Applications of Diamond*, Butterworth-Heinemann Ltd., Oxford, UK, 1991, pp. 468-481.

Wright, D. N., and H. Wapler, "Investigations and Prediction of Diamond Wear When Sawing," *Annals of the CIRP*, Vol. 35, No. 1, 1986, pp. 239-244.

Yang, C., H. D. Jerro, and S. S. Pang, "Finite Element Analysis of Segmented Circular Sawblades," *Conference Proceedings of the 1994 Science, Engineering, & Technology Seminars*, Houston, Texas, May 1994, pp. ME-II-14-18.

Other Pertinent Literature

Boyé, A., and P. Eglème, "Optimization of Sawing Conditions in Granite Cutting," in *New Developments in Grinding; Proceedings of the 1st International Grinding Conference*, ed. M. C. Shaw, Pittsburgh, 1972, pp. 870-887.

Büttner, A., "Coolant Additives in the Sawing of Granite," *Industrial Diamond Review*, Vol. 40, No. 9, 1980, pp. 332-335.

Chalkley, J. R., "The Tribological Aspects of Metal-Bonded Diamond Grinding Wheels," *Powder Metallurgy*, Vol. 12, No. 24, 1969, pp. 582-597.

Knowlton, R. H., and M. Russell, "Diamond Shape Technology Improves Cutting Structures," *Superabrasives Conference* 1991, pp. 3.9-3.21.

Konstanty, J. and A. Bunsch, "Hot Pressing of Cobalt Powders," *Powder Metallurgy*, Vol. 34, No. 3, 1991, pp. 195-198.

Levin, E., and E. Y. Gutmanas, "Solid-State Bonding of Diamond to Nichrome and Co-20 wt% W Alloys," *Journal of Material Science Letters* 9, 1990, pp. 707-710.

Liao, T. W., G. Sathyanarayanan, L. J. Plebani, M. U. Thomas, and K. Li, "Characterization of Grinding-Induced Cracks in Ceramics," *International Journal of Mech. Science*, Vol. 37, No. 9, 1995, pp. 1035-1050.

Lin, Z., and A. Queeney, "Fracture Resistance of Diamond-Reinforced Hot Pressed Cu/Ni Powders," *Powder Metallurgy International*, Vol. 18, No. 2, 1986, pp. 76-78.

Mamalis, A. G., H. Tönshoff, and R. Schulze, "The Static Compression of Solid Spheres of Hard Rock," *Res Mechanica*, Vol. 1, No. 1, Sept. 1980, pp. 265-275.

Outwater, J. O., "Surface Temperatures in Grinding," *Tranactions of the ASME*, Vol. 74, No. 1, 1959, pp. 73-86.

Pai, D. M., E. Ratterman, and M. C. Shaw, "Grinding Swarf," *Wear*, Vol. 131, 1989, pp. 329-339.

Rubenstien, C., "The Mechanics of Grinding," *Int. J. Mach. Tool Des. Res.*, Vol. 12, 1972, pp. 127-139.

Schiller, Z., N. Gross, and L. Driscoll, "Diamonds and Dirt," *Business Week*, August 10, 1992, pp. 20-23.

Tönshoff, H., N. Schmidt, and W. Ertingshausen, "A New Machine Concept for Deep Sawing Concrete," translation from *Industrie Diamanten Rundschau* 1983 No. 1., pp. 4-10.

Voyiadjis, G. Z., and M. Foroozesh, "A Finite Strain, Total Lagrangian Finite Element Solution for Metal Extrusion Problems," *Computer Method in Applied Mech. and Engr.*, 86, 1991, pp. 337-370.

Zienkiewicz, O. C., *The Finite Element Method: Basic Formulation and Linear Problems, Vol. 1.*, McGraw-Hill Book Co., Europe, 1987.

Zienkiewicz, O. C., *The Finite Element Method: Solid and Fluid Mechanics, Dynamics and non- Linearity*, Vol. 2, 4th Ed., McGraw-Hill Book Co., Europe, 1991.

APPENDIX A

CHIP ARC LENGTH TO BLADE DIAMETER RATIO

Table Contains l_c/D Values

K_1	Developed Model K_2 Values							Slender Triangle Approximation Model
	0.00011	0.00040	0.00116	0.00192	0.00268	0.00344	0.00420	--
0.00	0.00000	0.00000	0.00000	0.00000	0.00000	0.00000	0.00000	0.00000
0.01	0.10018	0.10020	0.10027	0.10034	0.10041	0.10048	0.10055	0.10000
0.02	0.14191	0.14195	0.14204	0.14213	0.14222	0.14232	0.14241	0.14142
0.03	0.17410	0.17414	0.17425	0.17436	0.17447	0.17458	0.17469	0.17321
0.04	0.20138	0.20142	0.20155	0.20167	0.20179	0.20191	0.20204	0.20000
0.05	0.22553	0.22558	0.22572	0.22585	0.22599	0.22612	0.22625	0.22361
0.06	0.24749	0.24754	0.24768	0.24783	0.24797	0.24811	0.24826	0.24495
0.07	0.26779	0.26784	0.26799	0.26814	0.26829	0.26844	0.26860	0.26458
0.08	0.28678	0.28684	0.28700	0.28715	0.28731	0.28747	0.28763	0.28284
0.09	0.30472	0.30478	0.30494	0.30510	0.30527	0.30543	0.30559	0.30000
0.10	0.32177	0.32184	0.32201	0.32218	0.32234	0.32251	0.32268	0.31623
0.11	0.33809	0.33816	0.33833	0.33850	0.33867	0.33885	0.33902	0.33166
0.12	0.35377	0.35383	0.35401	0.35419	0.35436	0.35454	0.35472	0.34641
0.13	0.36889	0.36896	0.36914	0.36932	0.36950	0.36968	0.36986	0.36056
0.14	0.38352	0.38359	0.38378	0.38396	0.38414	0.38433	0.38451	0.37417
0.15	0.39773	0.39780	0.39798	0.39817	0.39836	0.39854	0.39873	0.38730
0.16	0.41154	0.41162	0.41180	0.41199	0.41218	0.41237	0.41256	0.40000
0.17	0.42502	0.42509	0.42528	0.42547	0.42566	0.42585	0.42604	0.41231
0.18	0.43818	0.43825	0.43844	0.43864	0.43883	0.43902	0.43921	0.42426
0.19	0.45105	0.45113	0.45132	0.45152	0.45171	0.45191	0.45210	0.43589
0.20	0.46368	0.46375	0.46395	0.46414	0.46434	0.46453	0.46473	0.44721
0.21	0.47606	0.47614	0.47633	0.47653	0.47673	0.47692	0.47712	0.45826
0.22	0.48823	0.48831	0.48851	0.48870	0.48890	0.48910	0.48930	0.46904
0.23	0.50021	0.50028	0.50048	0.50068	0.50088	0.50108	0.50127	0.47958
0.24	0.51200	0.51208	0.51228	0.51247	0.51267	0.51287	0.51307	0.48990
0.25	0.52363	0.52370	0.52390	0.52410	0.52430	0.52450	0.52470	0.50000
0.26	0.53510	0.53518	0.53537	0.53557	0.53577	0.53597	0.53617	0.50990
0.27	0.54643	0.54650	0.54670	0.54690	0.54710	0.54730	0.54750	0.51962
0.28	0.55763	0.55770	0.55790	0.55810	0.55830	0.55850	0.55870	0.52915
0.29	0.56870	0.56878	0.56898	0.56918	0.56937	0.56957	0.56977	0.53852
0.30	0.57967	0.57974	0.57994	0.58014	0.58034	0.58053	0.58073	0.54772
0.31	0.59053	0.59060	0.59080	0.59100	0.59119	0.59139	0.59159	0.55678
0.32	0.60129	0.60137	0.60156	0.60176	0.60196	0.60215	0.60235	0.56569
0.33	0.61197	0.61204	0.61224	0.61243	0.61263	0.61282	0.61302	0.57446
0.34	0.62256	0.62264	0.62283	0.62302	0.62322	0.62341	0.62361	0.58310
0.35	0.63308	0.63315	0.63335	0.63354	0.63373	0.63392	0.63412	0.59161

APPENDIX B

DIAMOND SEGMENT PHOTOMICROGRAPHS

Wear Character of a Diamond Segment After 224 Hours of Work (460.1 m^2 Sawn) on Red Mahogany Granite at Milbank, South Dakota (Figures from Mirshams et al., 1994)

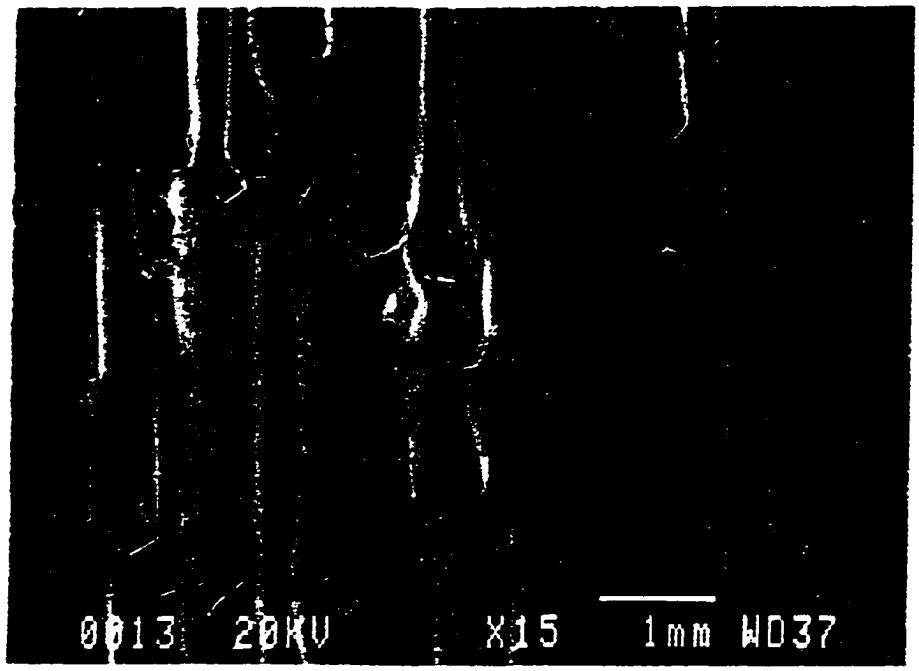

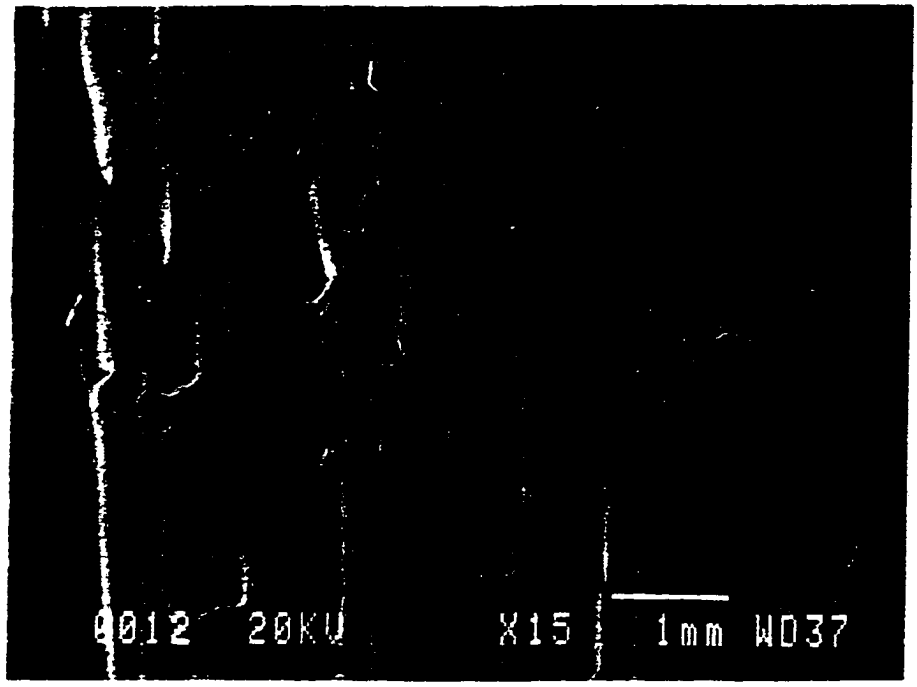

APPENDIX C

DIAMOND GRIT SPACING (DIGS) NUMERICAL COMPUTATION PROGRAM

C.1 Program Flow Chart

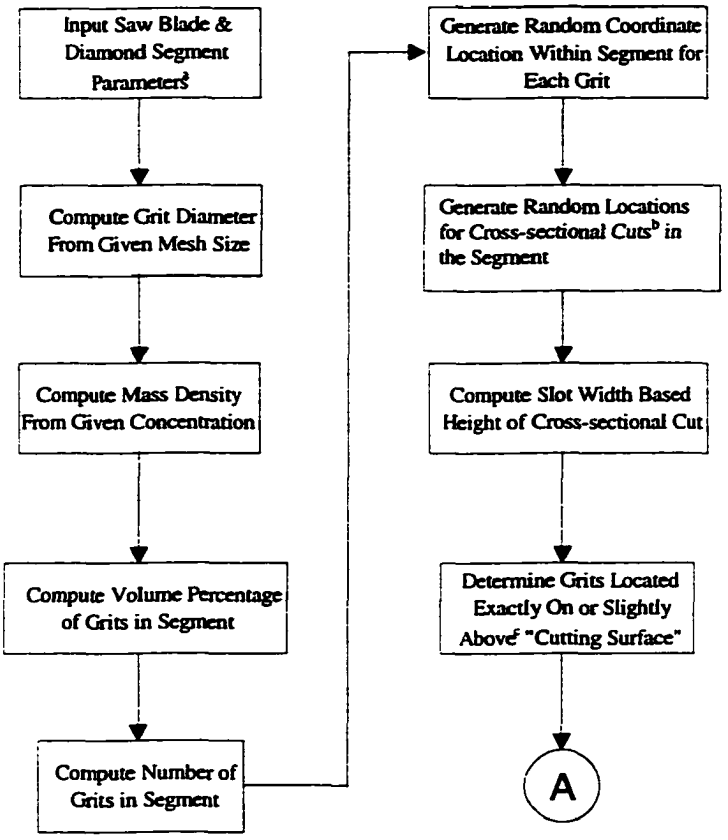

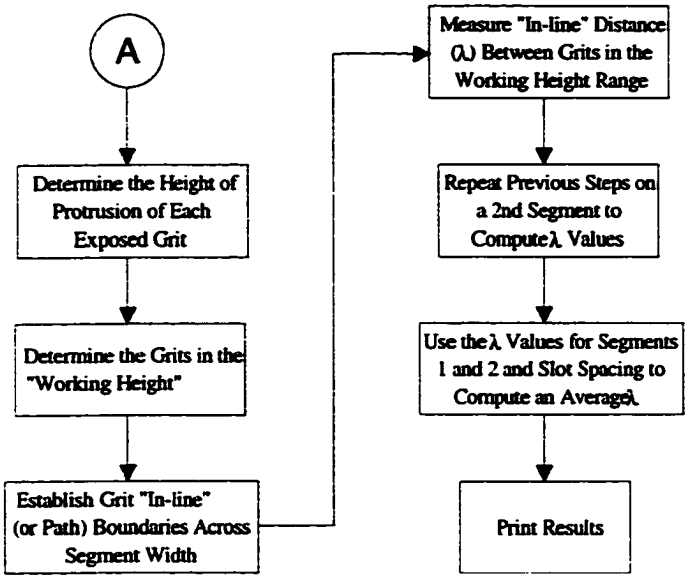

Notes:

[b]: Each cut represents the actual "cutting surface."

[c]: Slightly above means no more than 40% of the diamond is above the cutting surface.

[a]: Input Parameter List:

Dnb	=	nominal blade diameter
Nseg	=	number of segments on the blade periphery
Lseg	=	length of one diamond segment
Wseg	=	width of segment
Hseg	=	height of segment
Conc	=	grit concentration in segment matrix
Msiz	=	US Mesh size of grit
Dens	=	density of diamond

C.2 Program Flow Source Code

```
C ***************************************************************************
C ***************************************************************************
C   Diamond Grit Spacing (DiGS) Program
C   Written by H. Dwayne Jerro
C   Composite Materials Laboratory
C   Department of Mechanical Engineering
C   Louisiana State University
C   Date: 11-20-95
C ***************************************************************************
C ***************************************************************************
      IMPLICIT REAL*8 (a-h,o-z)
      CHARACTER*1       yes, no, ctnswp
      CHARACTER*2       tmode,tmode2
      INTEGER           zero, Nseg
      INTEGER           igptr(5,200),nmexpg(5)
      INTEGER           lncont(200)
      INTEGER*2         tmphour, tmpminute, tmpsecond, tmphund
      INTEGER*2         tmphour2, tmpminute2, tmpsecond2, tmphund2
      REAL              ranval
      REAL*8            Dsb, Lseg, Wseg, Hseg, Conc
      REAL*8            Dens, maxvge, workgp
      REAL*8            Mgrits
      REAL*8            zlane(200)
      REAL*8            X(10000,3)
      REAL*8            Hslice(10), Lslot(10)
      REAL*8            hexpg(5,200)
      REAL*8            xexpg(5,200),yexpg(5,200),zexpg(5,200)
      REAL*8            xglobl(200,150)
      REAL*8            lamgsm,lamsum(200)
      REAL*8            lamlcl(200,200),lamavg(200),lambda
      tmphund = 0
C ***************************************************************************
C   Show current date and time.
C ***************************************************************************
      CALL GETTIM(tmphour, tmpminute, tmpsecond, tmphund)
      tmode = 'AM'
      IF(tmphour .GE. 12) THEN
            ihour  = tmphour - 12
            tmode = 'PM'
      ENDIF
      WRITE (*,1)'COMPUTATION START TIME --> ',ihour,':', tmpminute
     &      ,':' , tmpsecond,'.', tmphund,tmode
1     FORMAT(3x,a27,2x,i2,a1,i2,a1,i2,a1,i2,1x,a2,/)
      OPEN(Unit = 1, File='DIGSOUT\LAM40.OUT', Status = 'NEW')
      OPEN(Unit = 2, File='DIGSOUT\XYZ40.OUT', Status = 'NEW')
C ***************************************************************************
C     PROGRAM CONTANTS and LIMITS OF ARRAYS
C ***************************************************************************
C   pi:         Mathematical constant
C   maxnmg:     Maximum number of grits in a segment
```

```
C    maxnmln:   Maximum number of cutting lanes in a segment (z-direction)
C    maxnmc:    Maximum number of cuts or "slices" (y-direction)
C    maxsfg:    Maximum number of surface grits in a "slice"
C    maxnmp:    Maximum number of paths across width of segment
C    maxwgp:    Maximum number of working grits per path
C    zero:      Mathematical or logical constant
C ***************************************************************************
      pi    = 3.141593d0
      maxnmg = 10000
      maxnmln= 200
      maxnmc = 1
      maxsfg = 400
      maxnmp = 100
      maxwgp = 10
      zero  = 0
      Ntestg = 1500
C ***************************************************************************
C     The initial seed value for the random number generator is given.
C ***************************************************************************
      iseed  = tmphund
      write(*,*) 'random time seed =',iseed
C ***************************************************************************
C      DIAMOND SEGMENT and GRIT PROPERTIES
C ***************************************************************************
C    Dsb:       Diameter of saw blade (segment height not included) (mm)
C    Nseg:      Number of segments on periphery of saw blade
C    Lseg:      Length of segment (mm)
C    Wseg:      Width of segment (mm)
C    Hseg:      Height of segment (mm)
C    Conc:      Concentration of diamond grit in segment matrix
C               (Units -> 100 Conc = 4.4 carats/cm^3)
C    Msiz:      Mesh (or sieve) size in US Mesh units (ANSI B74.16-1971)
C    Dens:      Density of diamond (gm/cm^3)
C    maxvge:    Maximum volume percentage of grit exposed
C    workgp:    Percentage of working grits
C    convr1:    Mass conversion factor (gm/carat)
C    convr2:    Concentration conversion factor (carat/cm^3)/conc. unit
C ***************************************************************************
      Dsb   = 390.0d0
      Nseg  = 24
      Lseg  = 40.0d0
      Wseg  = 2.8d0
      Hseg  = 10.0d0
      Dens  = 3.515d0
      maxvge = 40.0d0
      workgp = 25.0d0
      convr1 = 0.20d0
      convr2 = 0.044d0
      DO 4 i = 1,2
            WRITE(i,3)'Blade Diameter =',Dsb,'mm','Num of Segments =',
     *      Nseg,'Segment Length =',Lseg,'mm','Segment Width  =',Wseg
     *      ,'mm','Segment Height =',Hseg,'mm'
3           FORMAT(1x,a17,f6.1,1x,a2,/
     *      1x,a17,i3,/,
     *      1x,a17,f5.1,1x,a2,/,
```

```
     *          1x,a17,f5.1,1x,a2,/,
     *          1x,a17,f5.1,1x,a2)
4         CONTINUE
          WRITE(*,*) 'INPUT STARTING CONCENTRATION & PRESS ENTER: '
          READ(*,*) ksta
          WRITE(*,*) 'INPUT ENDING CONCENTRATION & PRESS ENTER: '
          READ(*,*) kend
          WRITE(*,*) 'INPUT DESIRED MESH SIZE AND PRESS ENTER: '
          READ(*,*) Msiz
          DO 9000 iConc = ksta,kend,5
C *************************************************************************
C     Convert Concentration to Mass Per Unit Volume Units (gm/cm^3)
C *************************************************************************
                    Conc  = iConc*1.0d0
                    Conc  = Conc*convr1*convr2
C *************************************************************************
C                   Compute Average Diameter of Grits (um)
C *************************************************************************
C                   Msiz  = 40
                    CALL GRTSIZ(Msiz,dgrit)
                    WRITE(*,*)'Concentration  = ',Conc/convr1/convr2,' units ='
                    WRITE(*,*)'US Mesh Size   = ',Msiz
C *************************************************************************
C     Compute Volume and Mass of Grits and Segment
C *************************************************************************
C   Vseg:       Volume of the composite segment (cm)
C   Mgrits:     Total mass of the grits in the segment (gm)
C   Vgrits:     Total volume of the grits in the segment (cm^3)
C   Vpcent:     Volume percentage of grits in segment (%)
C   V1g:        Volume of one spherical grit (cm^3)
C   V1gum:      Volume of one spherical grit (um^3)
C   delpmx:     Maximum protrusion height (um)
C   delpmin:    Minimum protrusion height (um)
C   delct:      Average cut thickness (um)
C   delcw:      Average cut width (um)
C   pconst:     Protrusion constant (mm)
C   tweakf:     Tweak factor representing space between adjacent grits (um)
C *************************************************************************
                    Vseg  = (Lseg*Wseg*Hseg)/1000.0d0
                    Mgrits = Vseg*Conc
                    Vgrits = Mgrits/Dens
                    Vpcent = (Vgrits/Vseg)*100.0d0
                    V1g   = (pi/6.0d0)*(dgrit/10000.0d0)**3.0
                    V1gum = (pi/6.0d0)*(dgrit)**3.0
                    DO 8 i = 1,2
                         WRITE(i,6)'US Mesh Size   = ',Msiz,'Grit Diameter  = ',dgrit
     *                   ,'um','*************************************************',
     *                   'Concentration  = ',Conc/convr1/convr2,'units =',
     *                   Conc,'gm/cm^3'
6                        FORMAT(1x,a18,i2,/,1x,a18,f5.1,1x,a2,/,///,a50,/
     *                   1x,a18,f5.1,1x,a7,f8.5,1x,a7)
                         WRITE(i,7)'Total Vol of Grits   --> Vg  =',Vgrits,' cm^3',
     *                   'Vol% of Grits in Seg  --> V%  =',Vpcent,' %',
     *                   'Grit Vol% Exposed     --> Vpe =',maxvge,' %',
     *                   'Grit % @ Work Height  --> Pwh =',workgp,' %'
```

```
7                   FORMAT(1x,a31,f8.5,a5,/,
     *              1x,a31,f8.4,a2,/,
     *              1x,a31,f7.2,a2,/,
     *              1x,a31,f7.2,a2)
8             CONTINUE
C ***************************************************************************
C    Compute Number of Grits in Segment Using Initial Data
C ***************************************************************************
              Ngrits = NINT(Vgrits/V1g)
              DO 10 i = 1,2
                   WRITE(i,9)'Total Num of Grits   --> Ngr =',Ngrits
9                  FORMAT(1x,a31,i5/)
10            CONTINUE
C ***************************************************************************
C    Determine the maximum protrusion height relative
C    to the reference datum in which a grit can be
C    exposed to the surface.
C ***************************************************************************
              temp1  = 1.0d0/3.0d0*dacos(1.0d0 - maxvge/50.0d0)
              delpmx = dgrit*(0.5d0 + dcos(temp1 + 4.0d0*pi/3.0d0))
C ***************************************************************************
C    Determine the minimum protrusion height delpmin whereby cutting will occur
C    Also, the average thickness of cut delct and the average width of cut delcw
C    is computed.
C ***************************************************************************
              delpmin = (1.0d0 - workgp/100.0d0)*delpmx
              delct   = (delpmx - delpmin)/2.0d0
              delcw   = 2.0d0*DSQRT((dgrit-delct)*delct)
C ***************************************************************************
C    Protrusion constant is used to insure that more than
C    the maximum allowable amount of grit volume is not
C    protruding from the edges of the composite segment.
C ***************************************************************************
              pconst = (dgrit/2.0d0 - delpmx)/1000.0d0
C ***************************************************************************
C    Compute the maximum number of lateral cutting lanes which are
C    permitted with the given segment width.
C    The grit "in-line" path boundary (or limits) are also computed
C    for each lane.
C    Finally, the seed value for the random number generator is given.
C ***************************************************************************
C             zInsta:    width of cut boundary for first lane (um)
C             zlane(n):  width of cut boundary for each lane (um)
C ***************************************************************************
              nmlane  = INT((Wseg*1000.0d0)/delcw)
              zInsta  = (Wseg*1000.0d0 - nmlane*delcw)/2.0d0
              DO 12 i = 1,2
                   WRITE(i,11)'Max Protrusion Height --> dpmx =',delpmx,' um',
     *             'Min Protrusion Height --> dpmn =',delpmin,' um',
     *             'Grit Cut Thickness   --> delct =',delct, ' um',
     *             'Grit Cut Width       --> delcw =',delcw, ' um',
     *             'Protrusion Constant  --> pcons =',pconst*1000.0d0,
     *             ' um','Z Lane Start        --> zlans =',zInsta,' um',
     *             'Number of Lanes      --> nmlan =',nmlane
11                 FORMAT(1x,a32,f8.3,a3,/,
```

```
*                     1x,a32,f8.3,a3,/,
*                     1x,a32,f8.3,a3,/,
*                     1x,a32,f8.3,a3,/,
*                     1x,a32,f8.3,a3,/,
*                     1x,a32,f8.3,a3,/,
*                     1x,a32,i4)
12              CONTINUE
                DO 13  n = 1,(nmlane + 1)
                        zlane(n) = zlnsta + (n - 1)*delcw
13              CONTINUE
C ***************************************************************************
C  Generate a random cut positions along height of segment
C  Also note that each cut height will produce a different slot length
C  due to the fact that the arc length increases as the radius increases.
C ***************************************************************************
C   htinit:     (mm)
C   rgritm:     radius of grit (mm)
C   rgritu:     radius of grit (um)
C   irndct:
C   Hslice:     (mm)
C   Dnom:       (mm)
C   Lslot:      (mm)
C   toplim:     (mm)
C   botlim:     (mm)
C ***************************************************************************
                DO 7000  irndct = 1, maxnmc
C ***************************************************************************
C    Initialize the lane counting array, lncont(nlan) (i.e., set all its
C    values to zero). This variable keeps track (or counts) how many grits
C    fall in a respective lane.
C ***************************************************************************
      DO 14  nlan = 1,maxnmln
        lncont(nlan) = 0
14     CONTINUE
       rgritu = dgrit/2.0d0
                        rgritm = (dgrit/2.0d0)/1000.0d0
                        htinit = rgritm + Pconst
C                       CALL rand(ranval,iseed)
C                       Hslice(irndct) = ranval*(Hseg-Pconst-htinit)+htinit
                        Hslice(irndct) = 5.0d0
                        Dnom = Dsb + 2.0d0*Hslice(irndct)
                        Lslot(irndct) = pi*Dnom/Nseg - Lseg
      DO 17 i = 1,2
          WRITE(i,16)'Cut(or Slice) Height --> Hslic =',Hslice(irndct),
*       ' mm','Nominal Diameter    --> Dnom  =',Dnom,' mm',
*           'Slot Length @ Cut Ht --> Lslot =',Lslot(irndct),
*       ' mm'
16     FORMAT(3(1x,a32,f8.3,a3,/))
17     CONTINUE
C ***************************************************************************
C    Next determine the top and bottom limits for the center of the grits
C ***************************************************************************
                        toplim = Hslice(irndct) - Pconst
                        botlim = Hslice(irndct) - rgritm
C ***************************************************************************
```

```
C     Begin the loop to analyze the grit spacing in each segment which lies
C     of the periphery of the diamond saw blade.
C ***************************************************************************
      DO 5000 isegno = 1,Nseg
C      DO 5000 isegno = 1,5
C ***************************************************************************
C     Initialize the X(grit,coord) array (i.e., set all its values to zero).
C ***************************************************************************
         DO 20 icoord = 1,3
           DO 18 jgrit = 1,maxnmg
                                X(jgrit,icoord) = 0.0d0
18           CONTINUE
20         CONTINUE
C       GOTO 9999
C ***************************************************************************
C     Generate x, y, and z Coordinate Values for Each Grit
C     in the Diamond Segment Using the Random Number Generator
C ***************************************************************************
                    c     = pconst
                    idmcnt = 0
                    tweakf = 0.5d0
                    DO 200 igrit = 1, Ngrits
C                   DO 200 igrit = 1, 2000
25          CALL rand(ranval,iseed)
                               X(igrit,1) = pconst + (Lseg - 2*pconst)*ranval
                               CALL rand(ranval,iseed)
                               X(igrit,2) = pconst + (Hseg - 2*pconst)*ranval
                               CALL rand(ranval,iseed)
                               X(igrit,3) = pconst + (Wseg - 2*pconst)*ranval
C ***************************************************************************
C     Check to insure that none of the grits are overlapping by
C     using the distance between two points in space equation.
C     If this distance is less than dgrit for two grits, then
C     generate another random position for the new grit.
C ***************************************************************************
                               IF(igrit .GT. 1) THEN
                                       revdir = 1.0d0
                                       icount = 0
50             icount = icount + 1
                                       DO 100 k = (igrit - 1), 1, -1
                                               dx = (X(igrit,1)-X(k,1))*1000.0d0
                                               dy = (X(igrit,2)-X(k,2))*1000.0d0
                                               dz = (X(igrit,3)-X(k,3))*1000.0d0
                                               adx = dabs(dx)
                                               ady = dabs(dy)
                                               adz = dabs(dz)
                                     dist = DSQRT(adx**2.0d0 + ady**2.0d0 +adz**2.0d0)
                                               IF(dist .LT. dgrit) THEN
                                                  deld  = dgrit - dist + tweakf
                                                  deldx  = deld*(dx/dist)*revdir
                                                  deldy  = deld*(dy/dist)*revdir
                                                  deldz  = deld*(dz/dist)*revdir
                                                  X(igrit,1) = X(igrit,1) + deldx/1000.0d0
                                                  X(igrit,2) = X(igrit,2) + deldy/1000.0d0
                                                  X(igrit,3) = X(igrit,3) + deldz/1000.0d0
```

```
                IF(icount .gt. 100) revdir = -1.0d0
                    IF(icount .gt. 200) GOTO 25
                    GOTO 50
                  ENDIF
                  revdir = 1.0d0
100         CONTINUE
C ***************************************************************************
C       Check to insure that the grit coordinate is within the segment
C       limits, that is, length, width, and height.
C ***************************************************************************
                  IF((X(igrit,1).LT.c).OR.(X(igrit,1).GT.(Lseg-c)))
     *      THEN
              idmcnt = idmcnt + 1
                    GOTO 25
                  ELSEIF((X(igrit,2).LT.c).OR.(X(igrit,2).GT.(Hseg-c)))
     *      THEN
            idmcnt = idmcnt + 1
                    GOTO 25
                  ELSEIF((X(igrit,3).LT.c).OR.(X(igrit,3).GT.(Wseg-c)))
     *      THEN
                    idmcnt = idmcnt + 1
                    GOTO 25
                  ENDIF
                      ENDIF
200     CONTINUE
                WRITE(*,*)isegno,' SEGMENT(S) COMPLETED',
     *        ' Dummy Grits =',idmcnt
C ***************************************************************************
C     Determine which grits belong in the exposed surface designation
C     for the respective random cut.
C ***************************************************************************
                  iegcnt = 0
                  DO 300 igrit = 1, Ngrits
                    ygtval = X(igrit,2)
                    IF((ygtval .LE. toplim).AND.(ygtval .GT. botlim)) THEN
                      hexpos = rgritu - (Hslice(irndct)-ygtval)*1000.0d0
                      iegcnt = iegcnt + 1
                      igptr(irndct,iegcnt) = igrit
                      hexpg(irndct,iegcnt) = hexpos
                      xexpg(irndct,iegcnt) = X(igrit,1)
                      yexpg(irndct,iegcnt) = X(igrit,2)
                      zexpg(irndct,iegcnt) = X(igrit,3)
C                     IF(irndct.eq.4) then
C                       WRITE(*,275) 'ig=', igrit,'ieg=',iegcnt,hexpos
C275            FORMAT(2x,a5,3x,i5,3x,a5,3x,i5,3x,f10.4)
C                     ENDIF
                    ENDIF
300       CONTINUE
                  nmexpg(irndct) = iegcnt
C ***************************************************************************
C     Sorting routine which orders surface grits from largest to
C     smallest protrusion height
C ***************************************************************************
                  yes = '1'
                  no  = '0'
```

```
                    DO 600  kswap = 1, 10*nmexpg(irndct)
                      ctnswp = no
                      DO 500  i = 1, (nmexpg(irndct) - 1)
                        IF(hexpg(irndct,i) .LT. hexpg(irndct,i+1)) THEN
                          CALL SWAPR8(hexpg(irndct,i),hexpg(irndct,i+1))
                          CALL SWAPR8(xexpg(irndct,i),xexpg(irndct,i+1))
                          CALL SWAPR8(yexpg(irndct,i),yexpg(irndct,i+1))
                          CALL SWAPR8(zexpg(irndct,i),zexpg(irndct,i+1))
                          CALL SWAPI(igptr(irndct,i),igptr(irndct,i+1))
                        ctnswp = yes
                        ENDIF
500           CONTINUE
                      IF(ctnswp.EQ.no) GOTO 690
600         CONTINUE
690         WRITE(2,692)'*** SEGMENT #',isegno,'***','no.','delp(um)',
     *            'x(mm)','y(mm)','z(mm)'
692         FORMAT(/,5x,a13,i2,a3,/,3x,a3,3x,2x,a8,3(3x,5x,a5,1x))
          DO 695 jj = 1, nmexpg(irndct)
            mm = irndct
                      WRITE(2,693) jj,hexpg(irndct,jj),
     *                xexpg(mm,jj),yexpg(mm,jj),zexpg(mm,jj)
693           FORMAT(1x,i4,4(3x,f11.5))
695         CONTINUE
C ***************************************************************************
C     The number of working grits for the given cut is computed.
C     Then the qualifying grits are tested to determine which lane the grit
C     should be placed.
C ***************************************************************************
          nmwg = NINT(nmexpg(irndct)*workgp/100.0d0)
         WRITE(2,698)'**** Number of Exposed Grits =',nmexpg(irndct)
     *       ,' ****','**** Number of Working Grits =',nmwg,' ****'
698         FORMAT(1x,a31,i4,a5,/,1x,a31,i4,a5)
DO 810 mgrit = 1,nmwg
           DO 800 nlan = 1,nmlane
          IF(zexpg(irndct,mgrit).GE.(zlane(nlan)/1000.0d0).AND.
     *         zexpg(irndct,mgrit).LT.(zlane(nlan+1)/1000.d0)) THEN
            lncont(nlan) = lncont(nlan) + 1
            xglobl(nlan,lncont(nlan)) = (isegno - 1)*(Lseg
     *          + Lslot(irndct)) + xexpg(irndct,mgrit)
GOTO 810
           ENDIF
800        CONTINUE
810       CONTINUE
5000     CONTINUE
C ***************************************************************************
C     The qualifying grits are now sorted from largest x distance to
C     the smallest x position for each individual lane.
C ***************************************************************************
         lamgsm = 0.0d0
         lamcnt = 0
         DO 1300 nlan = 1,nmlane
                    DO 1000  kswap = 1, 10*lncont(nlan)
                      ctnswp = no
                      DO 900  i = 1, (lncont(nlan) - 1)
                        IF(xglobl(nlan,i) .LT. xglobl(nlan,i+1)) THEN
```

```
                        CALL SWAPR8(xglobl(nlan,i),xglobl(nlan,i+1))
                        ctnswp = yes
                      ENDIF
900          CONTINUE
                    IF(ctnswp.EQ.no) GOTO 1100
1000        CONTINUE
C ***************************************************************************
C     The local lambda values are computed for each two consecutive grits
C     in the given lane.
C ***************************************************************************

1100         WRITE(1,1110) '***** LANE #',nlan,' *****'
1110         FORMAT(/,1x,a12,i3,a6)
           lamsum(nlan) = 0.0d0
           DO 1200 num = 1, lncont(nlan)
             IF(num .LT. lncont(nlan)) THEN
               lamlcl(nlan,num) = xglobl(nlan,num)
     *                          -xglobl(nlan,num+1)
               lamsum(nlan) = lamsum(nlan) + lamlcl(nlan,num)
               WRITE(1,1150)num,xglobl(nlan,num),lamlcl(nlan,num)
1150             FORMAT(3x,i4,2(5x,f11.5))
             ENDIF
             IF(num .EQ. lncont(nlan)) THEN
               IF((lncont(nlan)-1).GT.0) THEN
                 lamavg(nlan) = lamsum(nlan)/(lncont(nlan)-1)
               ENDIF
               WRITE(1,1175) num,xglobl(nlan,num)
1175             FORMAT(3x,i4,5x,f11.5)
             ENDIF
1200         CONTINUE
           lamcnt = lamcnt + (lncont(nlan)-1)
           lamgsm = lamgsm + lamsum(nlan)

1300       CONTINUE

C ***************************************************************************
C     The overall lambda value is computed for all of the grits in each lane
C     and the results are printed to the output file as well as the lambda
C     averages for each lane.
C ***************************************************************************
                      lambda = lamgsm/lamcnt
                      DO 1400 i = 1,nmlane
                            IF(i. EQ. 1) THEN
                                  WRITE(1,1325) '****** LANE #  AVERAGE LAMBDA
     *                            (mm)',
     *                            '******'
1325                              FORMAT(/,1x,a35,1x,a6)
                                  ENDIF
                                  WRITE(1,1350) i,lamavg(i)
1350                              FORMAT(1x,6x,i4,6x,f11.5)
                                  IF(i .EQ. nmlane) THEN
                                  WRITE(1,1375)'****** GLOBAL LAMBDA
                      =',lambda,'mm',
     *                            '******'
1375                              FORMAT(/,3x,a22,f11.4,1x,a2,1x,a6,///)
```

```
                        ENDIF
1400                  CONTINUE
7000              CONTINUE
9000    CONTINUE
C ***************************************************************************
C     The following statements compute the elapsed time required to run this
C     program.  It uses the internal clock supplied by MS-DOS.
C ***************************************************************************
9999    CALL GETTIM(tmphour2, tmpminute2, tmpsecond2, tmphund2)
        WRITE (*,10000)'COMPUTATION START TIME  --> ',ihour,':',
   *    tmpminute,':' , tmpsecond,'.', tmphund,tmode
10000   FORMAT(3x,a27,2x,i2,a1,i2,a1,i2,a1,i2,1x,a2,/)
        tmode2 = 'AM'
        IF(tmphour2 .GE. 12) THEN
                ihour2 = tmphour2 - 12
                tmode2  = 'PM'
        ENDIF
        WRITE (*,10000)'COMPUTATION END TIME    --> ',ihour2,':',
   *    tmpminute2,':' , tmpsecond2,'.', tmphund2,tmode
        tm1 =tmphour*60.0+tmpminute+(tmpsecond+tmphund/100.0)/60.0
        tm2 =tmphour2*60.0+tmpminute2+(tmpsecond2+tmphund2/100.0)/60.0
        WRITE (*,*) ' Elapsed time...',(tm2-tm1),'minutes'
        STOP
        END

C ***************************************************************************
C     Subprogram which finds the average diameter of the grits
C     using the data provided by Sea Diamond Tools Technical
C     Product booklet.  Mesh (or sieve) size in US Mesh units
C     (ANSI B74.16-1971) and the diameter are in um units.
C ***************************************************************************
        SUBROUTINE GRTSIZ(Msiz,dgrit)
                REAL*8  dgrit
                INTEGER Msiz

                if(Msiz .eq. 10) dgrit = 2000.0d0
                if(Msiz .eq. 12) dgrit = 1680.0d0
                if(Msiz .eq. 14) dgrit = 1410.0d0
                if(Msiz .eq. 16) dgrit = 1190.0d0
                if(Msiz .eq. 18) dgrit = 1000.0d0
                if(Msiz .eq. 20) dgrit =  841.0d0
                if(Msiz .eq. 25) dgrit =  707.0d0
                if(Msiz .eq. 30) dgrit =  595.0d0
                if(Msiz .eq. 35) dgrit =  500.0d0
                if(Msiz .eq. 40) dgrit =  420.0d0
                if(Msiz .eq. 45) dgrit =  354.0d0
                if(Msiz .eq. 50) dgrit =  297.0d0
                if(Msiz .eq. 60) dgrit =  250.0d0
                if(Msiz .eq. 70) dgrit =  210.0d0
                if(Msiz .eq. 80) dgrit =  177.0d0
                if(Msiz .eq.100) dgrit =  149.0d0
                if(Msiz .eq.120) dgrit =  125.0d0
                if(Msiz .eq.140) dgrit =  105.0d0
                if(Msiz .eq.170) dgrit =   88.0d0
                if(Msiz .eq.100) dgrit =  149.0d0
```

```
            RETURN
        END

C ***************************************************************************
C     Subprogram which generates random numbers using the linear
C     congruential method of generating pseudorandom numbers.
C     Reference:  Fortran 77: Language and Style by Merchant
C           pp. 252-254
C ***************************************************************************
        SUBROUTINE rand(ranval,i)
            INTEGER i,j,k,m
            PARAMETER(j = 5243, k = 55397, m = 262139)
            i = MOD(i*j+k,m)
            ranval = (REAL(i)+0.5)/REAL(m)
            RETURN
        END

        SUBROUTINE SWAPR8(a,b)
            REAL*8  a,b,temp
            temp = a
            a = b
            b = temp
            RETURN
        END

        SUBROUTINE SWAPI(a,b)
            INTEGER  a,b,temp
            temp = a
            a = b
            b = temp
             RETURN
        END
```

APPENDIX D

LETTER OF PERMISSION

ASME International

212-591-7000
FAX 212-591-7674
www.asme.org

Three Park Avenue
New York, NY 10016-5990
U.S.A.

October 30, 1998

H. Dwayne Jerro
Department of Mechanical Engineering
Louisiana State University
Baton Rouge, LA 70803

Dear Mr. Jerro,

It is our please to grant you permission to include the following papers shown in your request of October 29, 1998:

1. Kinematics Analysis of Chipping Materials Using Superabrasive Diamond Tools, Proceedings of the ASME/ETCE 1995 Conference & Exhibition,

2. Kinematics of the Chipping Process Using Circular Diamond Saw Blades, by H. Jerro, S. Pang, C. Yang, and R. Mirshams, Journal of Manufacturing Science and Engineering.

3. Grit Distribution in Superabrasive Diamond Sawing, published in the 8th Annual Energy Week Conference & Exhibition Symp. on Composite Materials, Design and Analysis: Book IV, pp. 203-211.

We understand that this material will be included in your dissertation, "Characterization and Analysis of the Superabrasive Diamond Blade Sawing Process", at Louisiana State University. As is customary, we ask that full acknowledgment is provided to the authors, the source document, and ASME as original publisher.

Should you have any further question, please feel free to contact me.

Sincerely,

Philip V. DiVietro
Director
Technical Publishing
(P) 212-591-7696
(F) 212-591-7292
(E) divietrop@asme.org

cc: S. Pang

VITA

Harlan Dwayne Jerro was born on October 28, 1968, and is originally a native of Colfax, Louisiana. He graduated from Grant High School in 1986 with the honor of Salutatorian. He decided to pursue a Bachelor of Science Degree in Mechanical Engineering at the largest Afro-American university in the United States, Southern University and Agricultural and Mechanical College in Baton Rouge. After completing his undergraduate degree at Southern in December 1991, he entered the graduate program at one of Louisiana's most prestigious institutions of higher education, Louisiana State University Agricultural and Mechanical College in Baton Rouge. Mr. Jerro will receive a Doctor of Philosophy degree in Mechanical Engineering to be conferred in December 1998.

DOCTORAL EXAMINATION AND DISSERTATION REPORT

Candidate: Harlan Dwayne Jerro

Major Field: Mechanical Engineering

Title of Dissertation: Characterization and Analysis of the Superabrasive Diamond Blade Sawing Process

Approved:

Su-Seng Pang
Major Professor and Chairman

Dean of the Graduate School

EXAMINING COMMITTEE:

(Co-chair)

Date of Examination:

October 22, 1998

IMAGE EVALUATION
TEST TARGET (QA-3)

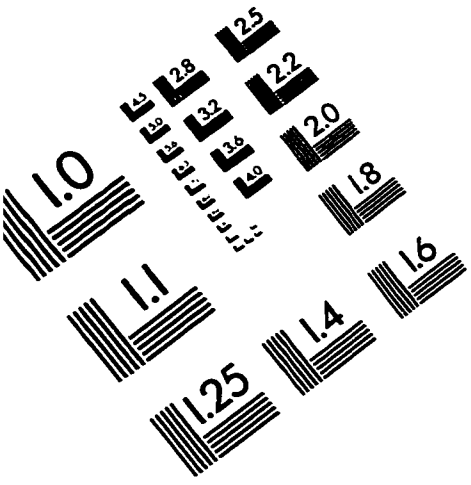

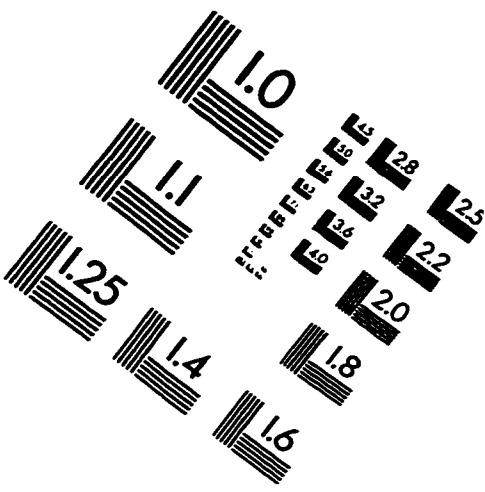

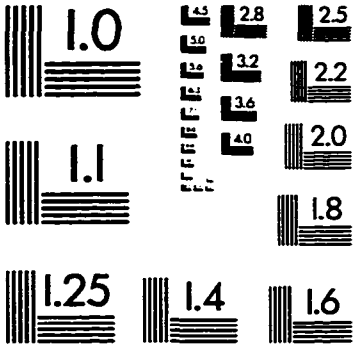

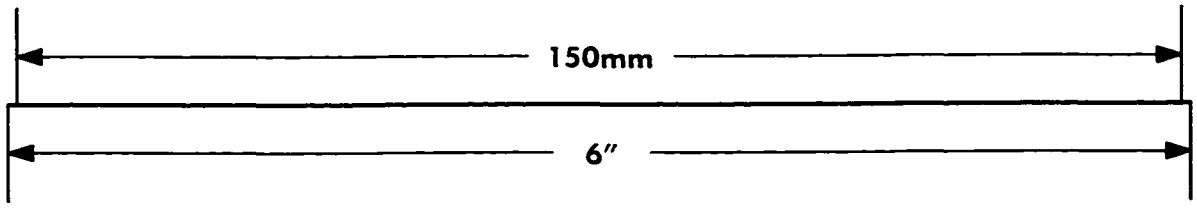

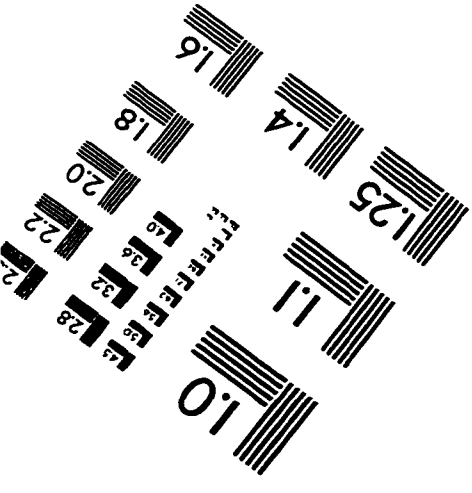

APPLIED IMAGE, Inc
1653 East Main Street
Rochester, NY 14609 USA
Phone: 716/482-0300
Fax: 716/288-5989